NUMERICAL SIMULATION OF FLOW AROUND A CIRCULAR CYLINDER

A Thesis submitted to

THAPAR INSTITUTE OF ENGINEERING & TECH. PATIALA

(DEEMED UNIVERSITY)

In partial fulfillment of the requirements for the

award of the degree of

MASTER OF ENGINEERING

IN

(CAD/CAM & ROBOTICS)

Submitted By:

NAVDEEP SINGH

Roll No. 8018110

Under the guidance of:

Dr. H.N. Chandrawat

Professor & Dean R.S.P.

Deptt. of Mechanical Engineering

T. I. E. T. Patiala

Under the guidance of:

Mr. Sumeet Sharma

Lecturer

Deptt. of Mechanical Engineering

T. I. E. T. Patiala

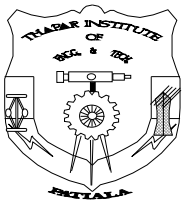

DEPARTMENT OF MECHANICAL ENGINEERING

THAPAR INSTITUTE OF ENGINEERING & TECHNOLOGY

(DEEMED UNIVERSITY)

PATIALA-147004, INDIA

2003

CERTIFICATE

This is to certify that the thesis entitled **"NUMERICAL SIMULATION OF FLOW AROUND A CIRCULAR CYLINDER",** being submitted by **Mr. NAVDEEP SINGH** in partial fulfillment of the requirements for the award of the degree of **MASTER OF ENGINEERING (CAD/CAM & ROBOTICS)** at **THAPAR INSTITUTE OF ENGINEERING & TECHNOLOGY (Deemed University), Patiala (India)**, is a bonafide work carried out by him under our supervision and guidance.

Dr. H.N. Chandrawat
Professor & Dean R.S.P.
Deptt. of Mechanical Engg.
Thapar Institute of Engg. and Tech.
Patiala-147004(Pb.)

Mr. Sumeet Sharma
Lecturer
Deptt. of Mechanical Engg.
Thapar Institute of Engg. and Tech.
Patiala-147004(Pb.)

(Dr. D. S. BAWA)
Dean, Academic Affairs.
THAPAR INSTITUTE OF ENGG. & TECH.
PATIALA-147004(PUNJAB)

(DR. R. G. TATHGIR)
Prof. & Head, MED.
THAPAR INSTITUTE OF ENGG. & TECH
PATIALA-147004(PUNJAB)

ACKNOWLEDGEMENT

I express my sincere gratitude to my guide **Dr. H.N. Chandrawat,** Professor and Dean RSP, Mechanical Engg. Department and **Mr. Sumeet Sharma**, lecturer, Mechanical Engg. Department, Thapar Institute of Engineering and Technology, for their valuable guidance, proper advice and constant encouragement during the course of my work on this thesis. They are a true guide in the sense that they generously gave me space to pursue my own ideas and make my own mistakes and take credit for my work.

I am deeply indebted to my parents for their inspiration and ever encouraging moral support, which enabled me to pursue my studies. I am also grateful to my brother-in-law and my sisters for their confidence and expectations from me, which I always strived to live up to.

I do not find enough words with which I can express my feelings of thanks to my dear friends Ajay Rana, Radhey Sham, Mayank, Rupesh, Vishal, Somesh, Kumar Gaurav, Munish, for their help, inspiration and moral support which went a long way in successful completion of present study.

I also extend my thanks to all the faculty and staff members of Mechanical Engg. Department for their direct and indirect help and cooperation.

(**NAVDEEP SINGH**)

8018110

ABSTRACT

A two dimensional numerical simulation of flow past a circular cylinder has been performed for a Reynolds number of 20. Navier-Stokes equations, the continuity equation in dimensionless form using velocity-pressure formulation are considered for the study of the both steady and unsteady flow problem. Finite element method using residual Galerkin method is used to solve the steady state flow problem. An explicit time marching scheme of approximate factorization for the solution of unsteady Navier-Stokes equations for the velocity field is used while the pressure field is computed from Poisson equation. Both studies show the presence of a two symmetrical wakes downstream attached to the cylinder and are in the close vicinity of the back of the cylinder. The wakes remain stable and do not shed vortices in the flow. Present computations for both the steady and unsteady problems are in good agreement with the experimental observations and the numerical calculations by several investigators.

INDEX

CONTENTS **PAGE NO.**

CHAPTER 1

INTRODUCTION

1.1 Introduction

A body placed in the flow field is of considerable interest as both the flow field and body interact with each other. The flow depends upon the shape of the body. It may be laminar or turbulent depending upon the body shape. Several problems involving the flow of fluid around submerged objects are encountered in the various engineering fields. Such problems may have either a fluid flowing around a stationary submerged object, or an object moving through a large mass of stationary fluid, or both the object and the fluid are in motion. Knowledge of forces exerted by the fluid on object is of significant importance in their design and analysis. The force exerted by the fluid on the moving body or on stationary body by fluid in motion can be resolved into two components, one in the direction of motion and other perpendicular to the direction of motion. The component parallel to the flow is called viscous drag and is due to the shear stress on the surface. The component perpendicular to the direction of motion of the flow is called pressure drag. This pressure drag tries to lift the body. However for a symmetric body, such as for a sphere or a cylinder, facing the flow symmetrically, there is no lift force and thus the total force exerted by the fluid is equal to the drag on the body.

The flow past a body is of direct relevance to the design of structures, heat exchanger components and where even flow induced vibration is important. The analysis of flow past a body in non-uniform stream is more complex. The approaching flow of a curved river against the bridge pier is one such example. Submarines, ships, aircraft, automobiles and missiles are examples where the object is in motion and the fluid is stationary. High rise buildings, chimneys and tube banks of heat exchangers are examples where the fluid is in motion. It is important to know the velocity, pressure and temperature fields in detail in a large

number of applications involving fluids, namely, liquid and gases. The performance of devices such as turbo-machinery and heat exchangers is determined entirely by the fluid motion within them and hence it is essential to know the pressure and velocity distribution to determine the effect on the body.

1.2 Flow around a circular cylinder

When a circular cylinder is placed in a fluid or the fluid flows around the cylinder there are a number of forces that are exerted on the cylinder namely pressure force, inertia force, viscous force, drag and lift. Fig. 1.1 shows flow past a circular cylinder placed in an infinite medium. The theoretical inviscid pressure distribution on the cylinder is shown by a firm line. Also P_∞ and U_∞ are the free stream pressure and velocity respectively. Considering the forces on the flow field, it is observed that in the inviscid region, the pressure and the inertia forces are in the same direction until $\theta=90^0$. Beyond $\theta=90^0$, the pressure gradient is positive and hence adverse. The pressure and the inertia forces oppose each other in the inviscid zone of this part of the cylinder. As long as no viscous effect is considered, the sum of potential and kinetic energy is preserved and the flow is completely reversed. When viscous forces are of considerable magnitude, until $\theta=90^0$ viscous forces oppose the combined effect of inertia and pressure forces. Fluid particles come across viscous resistance but they overcome it. Beyond $\theta=90^0$ inertia force is opposed by the pressure and viscous forces. Depending upon the magnitude of adverse pressure gradient, around $\theta=90^0$ (usually at an angle of 81^0 for a laminar boundary-layer) the fluid particles in the boundary layer are separated from the wall owing to the imbalance of pressure and inertia forces and is deflected in the upstream direction. The fluid particles beyond the point of separation follow the pressure gradient and move in a direction opposite to the external stream.

The point of separation is defined as the limit between forward and reverse flow in the layer in the immediate neighborhood of the wall,

i.e. at point of separation $\left.\frac{\partial u}{\partial y}\right|_{y=0} = 0$

Fig 1.1 Separation and interaction between viscous and inviscid regions

which implies that the shear stress at the wall, $\tau_\omega=0$.

Considering flow past a circular cylinder, near $\theta=90^0$ the boundary layer detaches itself from the wall and the pressure in the wake remains close to separation-point-pressure. The eddies (formed as a consequence of the retarded layers being carried along with the upper layer) cannot convert rotational kinetic energy into pressure head. The actual pressure distribution is shown by the dotted line in fig 1.1. Since the wake zone pressure is less than the pressure at the forward stagnation point (point A), the cylinder experiences a drag force. This drag force due to pressure difference is called form drag, whereas the shear stress at the wall gives rise to skin friction drag. The two drag forces are responsible for the resulting drag on the cylinder. As the base pressure decreases the recirculation region behind the cylinder becomes prominent. The recirculation region develops instabilities from the downstream end of the separation bubble, whose strength and amplification grows with Reynolds number.

At very low Reynolds number (≤1) the flow smoothly divides and reunites around the cylinder. At Reynolds number about 4, the flow separates in the downstream and wake zone is formed by two symmetrical standing eddies. Eddies remain steady but grow in size up to a Reynolds number of about 40. When the Reynolds number becomes about 40 eddies start to oscillate in time and thus brings asymmetry in the wake. Subsequently, the wake starts shedding vortices into the stream. This point is termed as onset of periodicity and the wake keep on undulating up to Reynolds number of 90. As the Reynolds number further increases the eddies are shed alternatively from the top and bottom of the cylinder and the regular pattern of alternatively shed clockwise and counter-clockwise toroidal vortices form a Von Karman vortex street (Fig 1.2d). At this stage periodicity is also induced in the flow due to the vortex shedding phenomenon. The periodicity is characterized by the frequency of vortex shedding f. In non-dimensional form, the vortex shedding frequency is expressed as fD/U, known as Strouhal number. The Strouhal number shows a slight but continuous variation with Reynolds number but is close to a value of

Fig 1.2 Influence of Reynolds number on wake zone aerodynamics

0.21. At about Re=500, multiple frequencies start showing up and the wake tends to become turbulent. The induced periodicity in the flow field culminates in periodic lateral forces on the cylinder. The cylinder starts vibrating and this phenomenon is known as flow-induced vibration. If the frequency of this forced vibration becomes equal to the natural frequency of the cylinder, the cylinder itself will collapse due to resonance.

Due to vortex shedding, the flow structure changes from steady to unsteady periodic, leading to a transition to turbulence. Till $\mathrm{Re} \leq 2\times10^5$ the boundary layer remains laminar and separation takes place at about 81^0 from the forward stagnation point. For larger Reynolds number the boundary-layer itself can become turbulent. A turbulent boundary layer offers greater resistance to separation than a laminar layer. Turbulence transmits kinetic energy from upper layers to the layers adjacent to the wall through the fluctuating transverse velocity component. As a consequence, the separation point moves downstream in a fully turbulent flow and separation is delayed to $\approx 110^0$ from the forward stagnation point. With further increase in Reynolds number the boundary layer on the cylinder itself becomes turbulent, separation occurs further upstream, yielding higher drag and base suction and a wider downstream wake than in the previous regime.

1.2.1 Wake Characteristics

The shape of the body and the wake generated by it as flow takes place around it are intimately related to each other. The wake is characterized by the following features.

Lift and Drag Coefficient: Any body immersed in a viscous fluid experiences a net force from shear stress and pressure difference caused by the motion of the fluid. Drag is the component parallel to and lift is component perpendicular to the flow direction. Drag and lift can be calculated from the experimentally derived coefficients, namely the lift coefficient and drag coefficient.

Drag coefficient is defined as

$$C_D = \frac{2F_D}{\rho V^2 A}$$

A is the drag generating area and $\frac{\rho V^2 A}{2}$ is dynamic pressure of stream. F_D is drag force. Lift coefficient is defined as

$$C_L = \frac{2F_L}{\rho V^2 A}$$

Vortex Shedding Frequency: In flow of fluids around objects and in the motion of bodies immersed in fluids, vibrations may occur because of formation of a wake caused by alternate shedding of eddies in a periodic fashion or by the vibration of the object. The dominant frequency in the wake and of the fluctuations in the lift and drag is specified by

$$S = \frac{fd}{U_\infty}$$

where f is measured in cycles per second, U_∞ is the free stream velocity and S is the Strouhal number.

Wake Size: It is characterized by the width of the wake, which depends upon the shape and size of the body and velocity of flow.

Evolution of Flow: This indicates the variation in spatial and time domain of pressure and velocity.

Vortical Structure and Time Traces: Vortical structure refers to the size and shape of the vortices and time trace refers to the variation of lift coefficient, drag coefficient and velocity with time. The bluff body is characterized by roll up of the separated shear layer. In two dimensional simulations, the vertices roll up very close bluff object. The vortex formation length is the distance beyond the bluff object along the wake centerline over which the stream wise component of velocity formation causes higher suction and thus higher drag.

1.3 Navier-Stokes Equations

In general form the two dimensional Navier-Stokes equations in X-direction can be written as:

$$\frac{Du}{Dt} = X - \frac{1}{\rho}\frac{\partial p}{\partial x} + \frac{\mu}{\rho}\left(\frac{\partial^2 u}{\partial x^2} + \frac{\partial^2 u}{\partial y^2}\right) \qquad \text{..... (1.1)}$$

In the above equation let us consider each term one by one.

$\frac{Du}{Dt}$ represent the total acceleration. It is the sum of the local and convective components. Now it can also be written as,

$$\frac{Du}{Dt} = \frac{\partial u}{\partial t} + u\frac{\partial u}{\partial x} + v\frac{\partial u}{\partial y}$$

$\frac{\partial u}{\partial t}$ represent the local contribution due to the change of velocity field with time at any position within the field. For steady state condition this component is zero.

$u\frac{\partial u}{\partial x} + v\frac{\partial u}{\partial y}$ represent the convective acceleration due to the movement of the particle through the velocity field.

X represents the x component of the body forces per unit mass acting on the flow.

$\frac{1}{\rho}\frac{\partial p}{\partial x}$ represent the pressure force acting on the fluid flow.

$\frac{\mu}{\rho}\left(\frac{\partial^2 u}{\partial x^2} + \frac{\partial^2 u}{\partial y^2}\right)$ represent the viscous shearing forces acting on the flow.

1.4 Approaches to Fluid Dynamical problems

The equations of fluid mechanics are known over a century but they can be solved for only a limited number of flows. The known solutions are useful only in solving fluid flow and cannot be used directly in engineering analysis or design. The most common approach used is the simplification of the equations using certain assumptions. These are usually based on a combination of approximations and dimensional analysis in which empirical input is almost always required. This approach is successful when the system can be described by one or two parameters so its applications to complex geometries are ruled out. A related approach is that for many flows non-dimensionalization of Navier-Stokes equations leaves the Reynolds number as the only independent parameter. If the body shape is held fixed, results can be get from an experiment

on a scale model with that shape. The desired Reynolds numbers are achieved by careful selection of the fluid and flow parameters. These approaches are very valuable and are the primary methods of practical engineering design everyday. The problem is that many flows require several dimensionless parameters for their specification and it may be impossible to set up an experiment which correctly scales the actual flow. Also sometimes experiments are very difficult if not possible. For example, the measuring equipment might disturb the flow or the flow may be inaccessible. Numerical methods came into existence as another alternative for solving flow problems with the birth of computers. Although many of the key ideas for Numerical solution methods for differential equations were established more than a century ago, they were of little use before computers appeared. Solution of the equations of fluid mechanics on computers has become very important and it now occupies the attention of all researchers in fluid mechanics. This field is known as computational fluid dynamics (CFD). Solution is obtained numerically by approximating the differential equations by using a discretization method, a system of algebraic equations are obtained which are then solved on a computer. The approximations are applied to small domains in space and time so the numerical solution provides results at discrete locations in space and time. So the solution is dependent on the quality of discretization used.

1.5 Need for Numerical Methods

Flow past bluff bodies has been studied extensively in the past. Depending upon the objectives, the numerical approach in some cases has been found to be more as appropriate compared to the experiments. For example for flows around aircraft or ships, in order to achieve the same Reynolds number with smaller models, fluid velocity has to be increased. For an aircraft this may give too high a Mach number if air is used. So there is need for a fluid which allows matching of both parameters. For ships, the issue is to match both the Reynolds number and Froude number, which is nearly impossible. With

numerical computations this is not difficult to as the boundary conditions can be easily prescribed for different cases.

In many cases experiments are very difficult if not impossible. For example the measuring equipment might disturb the flow or the flow may be inaccessible. (e.g. flow of a liquid silicon in a crystal growth apparatus). Some quantities are not measurable with present techniques or can be measured only with an insufficient accuracy. Experiments are an efficient means of measuring global parameters, like the drag, lift, pressure drop, heat transfer coefficients but in many cases details are important. It may be essential to know whether flow separation occurs or whether wall temp exceeds some limit. With improvement in technology and increase in market competition more careful optimization of designs are required. Also new high-technology applications demand prediction of flow for which the database is insufficient, experimental development may be too costly or time consuming. Numerical calculations can produce large volume of data needed and also permits parametric studies to be carried out at low cost.

The branch of solving fluid mechanics problems using numerical methods is called Computational Fluid Dynamics (CFD). In CFD appropriate solution of fluid dynamic equations is obtained by discretizing the equations with an appropriate method which approximates the differential equations by a system of algebraic equations, which can be then solved on a computer. The approximations are applied to small domains in space and/or time. So the numerical solution provides results at discrete locations in space and time. Therefore, as the accuracy of the experimental data depends upon the quality of the tools used, the accuracy of the numerical solution depends upon the quality of the discretization used.

1.6 Components of a Numerical Solution Method

1.6.1 Mathematical Model: Mathematical model is the starting point of any numerical method. It consists of a set of partial differential or integro-differential equations and boundary conditions. The differential equations can be classified as elliptic, hyperbolic, and parabolic or

some combination of these three categories, such as ultrahyperbolic, elliptically parabolic, or hyperbolically parabolic etc. Let us consider a very general partial differential equation in two independent variables

$$A\frac{\partial^2\phi}{\partial x^2}+2B\frac{\partial^2\phi}{\partial x\,\partial y}+C\frac{\partial^2\phi}{\partial y^2}=D\left(x,y,\phi,\frac{\partial\phi}{\partial x},\frac{\partial\phi}{\partial y}\right)$$

where A, B, and C are functions of only x and y. the above equation can be linear or nonlinear, depending upon the form of the function D.

If $B^2-AC<0$, the equation is elliptic.

If $B^2-AC=0$, the equation is parabolic.

If $B^2-AC>0$, the equation is hyperbolic.

For parabolic and hyperbolic equations the solution domains are usually open, whereas for elliptic equations the solution domains are defined by a closed boundary. An appropriate model is chosen for the target application.

1.6.2 Discretization Method: After selecting the mathematical model, a suitable discretization method is chosen i.e. a method of approximating the differential equations by a system of algebraic equations for the variables at some set of discrete location in space and time. There are many approaches, but the most important are finite difference (FD), finite volume (FV) and finite element (FE) methods. Finite difference method is the oldest method foe the numerical solution of the PDE's. It is the easiest method to use for simple geometries. In this the solution domain is covered by a grid. At each grid point, the differential equation is approximated by replacing the partial derivatives by approximations in terms of the nodal values of the functions. The result is one algebraic equation per grid node, in which the variable value at that and a certain number of neighbor nodes appear as unknowns. It can be applied to any grid but on structured grids it is very simple and

effective. Finite volume method uses the integral form of the equations as its starting point. The solution domain is subdivided into a finite number of contiguous control volumes, and the equations are applied to each CV. At the centroid of each CV lies a computational node at which the variable values are to be calculated. Interpolation is used to express variable values at the CV surface in terms of the nodal values. Surface and volume integrals are approximated using suitable quadrature formulae. Algebraic equations are obtained for each CV, in which a number if nodal values appear. FV can accommodate any type of grid. FV approach is the simplest to understand and to program. Finite element method is similar to FV method in many ways. The domain is broken into a set of discrete volumes or finite elements that are generally unstructured. In 2-D they are usually triangles or quadrilaterals, while in 3-D they are tetrahedral or hexahedral. The distinguishing feature of FE method is that the equations are multiplied by a weight function before they are integrated over the entire domain. In the simplest FE method, the solution is approximated by a linear shape function within each element in a way that guarantees continuity of the solution across element boundaries. The approximation is then substituted into the weighted integral of the conservation law and the equations to be solved are derived by putting the derivative of each nodal value to zero. The result is a set of nonlinear algebraic equations. The main advantage of finite element method is its ability to deal with arbitrary geometries. Other methods, like boundary element method, spectral schemes and cellular automata are also used in CFD but their use is limited to special classes of problems.

1.6.3 Coordinate and Basic Vector System: The equations can be written in many different forms, depending on the coordinate system and the basis vectors used. For example one can select Cartesian, cylindrical, spherical, curvilinear orthogonal or non-orthogonal coordinate system, which may be fixed or moving. The choice depends on the target flow,

and may influence the discretization method and grid type to be used. Also the basis in which vectors and tensors will be defined (fixed or variable, covariant or contravariant, etc.) is selected. Depending upon this choice, the velocity vector and stress tensor can be expressed in terms.

1.6.4 Numerical Grid: The discrete locations at which the variables are to be calculated are defined by the numerical grid which is discrete representation of the geometric domain on which the problem is to be solved. It divides the solution domain into a finite number of sub-domains (elements, control volumes etc.). Some of the grids are structured (regular) grid, block structured grid, and unstructured grids etc. Regular or structured grids consist of the grid lines with the property that members of a single family do not cross each other and only once crosses each member of the other families. The position of each grid within the domain is uniquely identified by a set of two (in 2-D) or three (in 3-D) indices, e.g. $(i, \quad j, \quad k)$. This is the simplest grid. Each point has four nearest neighbors in two dimensions and six in three dimensions. Structured grids can only be used for geometrically simpler solution domains. In block structured grids, there is a two (or more) level subdivision of solution domain. On the coarse level, there are blocks which are relatively large segments of the domain and their structure may be irregular and they may or may not overlap. On the fine level (within each block) a structured grid is defined. Special treatment is necessary at block level. For very complex geometries, unstructured grids are used. They are the most flexible type of grids and can fit any arbitrary solution domain boundaries. They can be used with any discretization scheme, but they are best adapted to the finite volume and finite element approaches. The elements and control volume may have any shape and any number of neighbor elements or nodes. In general grids made of triangles and quadrilateral in 2D and tetrahedral or hexahedra in 3D are most often used.

1.6.5 Finite Approximations: After the choice of the grid type, the approximations to be used in the discretization process are selected. In a finite difference method, approximations for the derivatives at the grid points have to be selected. In a finite volume method, one has to select the method of approximating surface and volume integrals. In finite element method, functions and weighting functions are selected.

1.6.6 Solution Method: discretization yields a large system of non-linear algebraic equations. The method of solution depends on the problem. For unsteady flows, methods based on initial value problem for ordinary differential equations are used. At each time step an elliptic problem has to be solved. Steady flow problems are usually solved by pseudo-time marching or an equivalent iteration scheme. Since the equations are non-linear, an iteration scheme is used to solve them. The choice of the solver depends on the grid type and the number of nodes in each algebraic equation.

1.6.7 Convergence Criteria: Finally a convergence criterion for the iterative method is set. Usually there are two levels of iterations: inner iterations, within which the linear equations are solved, and outer iterations, that deal with the non-linearity and coupling of the equations. Deciding when to stop the iterative process on each level is important, both for accuracy and efficiency.

1.7 Possibilities and limitation of Numerical Methods

There are many problems associated with experimental work. Some of these are easily dealt with in CFD. For example, if we want to simulate flow around a moving car in a wind tunnel, car model is fixed and air is blown at it but the floor has to move at the air speed which is difficult to do. It is not difficult to do in numerical simulation as boundary conditions are easily prescribed in computations. So if we solve the unsteady Navier-Stokes equations accurately, a

complete data set can be obtained from which any quantity of physical significance can be derived.

These advantages of CFD are conditional on being able to solve the Navier-Stokes equations accurately, which is extremely difficult for many flows of engineering interest. Also for many phenomena (e.g. turbulence, combustion, multiphase flow) the exact equation are not available or numerical solution is not feasible. This makes introduction of models a necessity. Even if equations are solved exactly, the solution would not be a correct representation of reality. The reason for differences between computed results and reality are:

- The differential equations may contain approximations and idealizations.
- Approximations are made in the discretization process.
- In solving the discretized equations, iterative methods are used. Unless they are run for a very long time, the exact solution of the discretized equation is not produced.

CHAPTER 2

LITERATURE SURVEY

A lot of work has been done in the field of study of flow around a circular cylinder. But so far much of the work has been done experimentally and with the increase in power of computational speed and memory available work in the field of numerical simulation is being done. Here, the research work of various researchers who contributed to the study is presented.

2.1 Importance of flow around circular cylinder

The study of flow around a circular cylinder is important from the engineering view point. When a fluid flows around a circular cylinder or the cylinder flows through the fluid, due to the cylinder fluid interaction there occurs a force on the cylinder and also there is variation in the velocity and pressure distribution around the cylinder. Due to these variations there is difference in the heat transfer rates, cooling rates etc. from the surface of the cylinder. It is frequently necessary to calculate pressure drop, heat transfer rates from tube bundles in heat exchange equipment. Design of cooling towers and chimney require an estimate of wind load. For these reasons, cross flow past a cylinder is an extensively studied.

2.2 Historical Brief

Since the first extensive measurements of vortex shedding frequencies of the circular cylinder wakes by Roshko in 1954, two-dimensional (2-D) and three-dimensional (3-D) vortical instabilities in wakes have been a subject of interest to engineers as well as scientists for a great many years. An understanding of the complex flow behind a circular cylinder poses a great challenge. Circular cylinder wakes are complex, they involve the interaction of three shear layers in the same problem, namely a boundary layer, a separating free shear layer, and a wake.

A great deal of impetus in this area was triggered by the classical work of von Karman in 1912 who analyzed the stability of vortex street configurations and established a link between the vortex street structures and the drag on the body. This work came from some experiments conducted by Hiemenz in the Prandtl's laboratory in Göttingen, who interpreted wake oscillations from a cylinder as an artifact of the experimental arrangement. However, von Karman viewed the wake oscillations and alternate generation of vortices as an intrinsic phenomenon, and investigated the linear stability of point vortex configuration. He found two rows of opposite-signed vortices were unstable in both symmetric and antisymmetric configuration, with the exception of one specific antisymmetric geometry exhibiting neutral stability. The above stability analyses pertain to infinite vortex arrays in the absence of a body, but Karman relate these studies to the vortex formation or shedding right behind the generating body. He does not explain why vortex streets are generated at the body in the first place but suggested that if such a configuration is formed, it can be seen for a large distance downstream.
Gerrard (1966) gives some descriptive understanding of near wake formation. He suggested that a forming vortex draws the shear layer (of opposite sign) from the other side of the wake across the wake centerline, cutting of the supply of vorticity to the growing wake vortex. This process can be understood from the instantaneous-streamline patterns drawn by Perry et al (1982) shown in fig.2.1 at the start of motion, the wake cavity contains a symmetrical set of equal and opposite recirculating-flow regions on either side of the wake as in fig 2.1a. However, when the vorticities begin to shed, this cavity opens and instantaneous "alleyways" of fluid penetrate the cavity. To relate this process with Gerrard's interpretation, imagine the anticlockwise vortex A is growing in strength from (a) to (d). In sketch (e), a saddle point S forms at the lower side of the body, which cuts off any new supply of vorticity bearing fluid to vortex A and instead forms a new vortex at the body.

FIGURE 2.1 Model of vortex shedding using topology of instantaneous streamlines.

Past experiments on wakes of circular cylinders in a laminar flow have shown that the vortex shedding is two-dimensional only at low Reynolds numbers. On reaching a certain Reynolds number the vortex shedding becomes oblique, where the vortices are parallel to each other but inclined with respect to the cylinder axis. Vortex shedding from circular cylinders in nature or in laboratory always has three-dimensional effects. Even in ideal laboratory conditions, the cylinder must have ends and these disturb the two-dimensional character of the vortex shedding. Over a Reynolds numbers range of about $50<Re<150$, observations on circular cylinder contaminated by end effects have

shown that (i) the spanwise axes of the shed vortices are not parallel to the cylinder axis, (ii) the shedding frequency is a function of the shedding angle and (iii) the resulting S-R curve is not continuous. Roshko (1954) proposed an empirical relationship linking frequency of shedding and the free stream velocity for a circular cylinder as

$$St = 0{,}212 - 4.5/\mathrm{Re} \quad 50<\mathrm{Re}<150$$

Tritton (1959) found two Strouhal curves, a “low speed” mode and a “high speed” mode, separated by a discontinuity near Re=100. He did not link the appearance of the discontinuity to changes of the geometry of the shed vortices, but interpreted it as a transition in the nature of the flow instability from a vortex street originating in the wake to a vortex street originating in the immediate vicinity of the cylinder.

In many practical situations, the inflow stream is not uniform, but has some form of shear imposed along the axis of the body. Such a situation is relevance to the design of chimneys placed in the earth’s boundary layer, marine risers, tethered buoys, and pillars of offshore platforms. In comparison to uniform flow, effects of shear on the vortex shedding mechanisms are relatively less understood. Only a few studies have been done in which the shedding frequencies and drag forces have been measured. The most distinguishing feature observed for shear flow over a bluff body is the shedding of vortices of constant frequency. Much of the theoretical work has been based on simple oscillator models, with modifications to include effects of three-dimensional geometry or upstream flow. Masch and Moore (1960) and later Shaw and Starr (1972) measured experimentally the drag and Strouhal number for a circular cylinder in shear flow and within the accuracy of the experiment they did not showed any cellular shedding pattern.

Berger (1964) discovered a discontinuity around Re=130, but related the discontinuity to the turbulence level in the wind tunnel. Gaster (1969, 71) showed that the discontinuities could be caused by a slight shear in the approaching flow, or due to a slight taper of the cylinder. He studied flow over slender cones, as a simplified analogue of shear flow over uniform cylinders, and observed that there

exists a spanwise coupling between regions of different characteristic frequency that introduces some amount of amplitude modulation to the shedding vortices. He also proposed a simple model for three-dimensional vortex shedding using the Van der Pol equation with a chain of spanwise stiffness. However, later in experiments by Maull and Young (1973), Mair and Stansby (1975), and Peltzer (1982), they noticed a distinct cellular pattern consisting of cells of constant frequency.

Maull and Young (1973) confirmed the conclusions found by Gaster. Gerrard (1978) suggested that Strouhal discontinuity at Re=100 was related to the end of the regime of Reynolds number in which diffusion of vorticity plays a primary role in the vortex shedding. Slaouti and Gharib (1981) reported that even in a good quality flow and with a smooth and straight cylinder the shed vortices are influenced by the geometry at the cylinder ends. But Mathis et al (1984) supported Gaster's idea discontinuity due to slight shear in the approaching flow.

Mair and Stansby (1975) conducted experiments on cylinders of various cross-sections and aspect ratios. They suggested an upper limit to the spanwise size of the cells. The largest cell lengths observed have been usually in the range of 4D to 6D. They observed base pressure based on local velocity and found it constant along the span with variations only at the ends. For short cylinders the effects were more pronounced. Also it was observed that the base pressure coefficient based on mean velocity varied linearly for most of the span and did not show any cellular pattern. This observation was inconsistent with Maull and young (1973) who had earlier observed a definite variation of base pressure curve in the spanwise direction. The change in the slope was linked to the boundary of cells of constant frequency. Peltzer (1982) reported that the boundaries of the constant frequency cells, away from the ends, show some temporal variation. Griffin (1985) showed that for various experimental conditions, cellular shedding has been observed along with spanwise variation of base pressure. Williamson (1988b) demonstrated two different modes of 3-D shedding in wake transition involving vortex loops and streamwise vortex pairs. In mode A, primary vortices deform in a wavy fashion along length during the

shedding process. In mode B, at higher Reynolds number finer-scale streamwise vortex pairs are formed. In this case primary vortex deformation is more spanwise uniform than for mode A.

Braza et al (1986) studied the pressure and velocity field in the near wake of the cylinder. The Navier-Stokes equations and the continuity equation were written in velocity-pressure form and solved by a predictor-corrector pressure formulation using second order accurate finite volume scheme and an alternating-direction-implicit scheme. They found that the flow at Reynolds number of 20 and 40 the flow becomes stable at nearly time t=7 and 15 respectively. The flow pattern is also presented at Reynolds number of 100, 200 and 1000 and over a long physical time. They very well predicted the Holf bifurcation leading to vortex shedding. The results were in agreement with those from the experiments. Jackson (1987) studied the onset of periodic behavior in two-dimensional laminar flow past bodies of various shapes. He used unsteady Navier-Stokes equations in their non-dimensional form and Galerkin formulation of the finite element method.

Van Atta and Gharib (1987) showed that all discontinuities in the Strouhal-Reynolds numbers curve can be attributed to the flow induced vibrations of the cylinder. If the aspect ratio is not large enough, even with good flow conditions, minimizing the wall boundary-layer effect is difficult. Therefore they suggested that in many previous cylinder wake investigations with aspect ratio usually does not exceed 300; the wall condition interference might have effected the natural two-dimensional shedding. So even in clean flow conditions and with the absence of cylinder vibrations, eliminating the influence of the boundary layers on the wake of a cylinder is necessary to achieve two-dimensional vortex shedding.

Williamson (1988) showed that the Strouhal-Reynolds number curve has a single discontinuity and is not caused by any of the ideas suggested so far. He proposed that the discontinuity is caused by three dimensional effects and in particular due to the phenomenon of oblique vortex shedding, which is controlled

to some extent by the end conditions. He further proposed that if the oblique shedding data is changed to parallel shedding data using the equation,

$$S_0 = S_\theta / \cos\theta$$

then the curve becomes completely smooth and devoid of discontinuities and also defined a empirical Reynolds-Strouhal relation that closely defines the universal curve as

$$S = -3.3265/Re + 0.1816 + 1.6\times10^{-4}\ Re$$

Hammache and Gharib (1989,91) also observed that parallel shedding results in continuous St-Re curve using control cylinders and devised a relation for parallel shedding data points as

$$St = 0.212 - 5.35 / Re$$

and found that the relation is in good agreement with the results of Williamson as far as parallel shedding is concerned and attributed the discontinuities solely to geometrical and flow conditions at the ends of the cylinder.

Noack et al (1991) presented a model, similar to that proposed by Gaster (1971), for the spanwise cell formation in the near wake of the cylinder in the non-uniform flow at low Re (0 ~ 60). However the accuracy of the model is limited by the appropriate selection of the coupling coefficients. Lee and Budwig (1991) also found results in excellent agreement with those of Williamson. Barkley and Henderson (1996) found, from their 2-D computations, that a very good fit for the St vs. Re data up to Re = 1000 is given by

$$St = 0.2417 - 0.8328\ Re^{-0.4808} \exp(-0.001895\ Re)$$

suggesting that an asymptote of 0.2417 is reached at large Re.

Balasubramaniam and Skop (1996) developed an elastically coupled Van der Pol oscillator model using a diffusive coupling in the spanwise direction. Their model closely replicates the cellular nature of vortex shedding observed in experiments. Anderson and Szewcayk (1996) investigated the concept of universal Strouhal parameter that would remain invariant for a variety of bluff bodies and flow configurations, including shear in the upstream flow and investigated different dimensionless groupings of base pressure, wake width, and Strouhal number.

Mukhopadhydy, Venugopal and Vanka (1999) used second order accurate finite volume scheme to integrate the unsteady Navier-Stokes equations and studied the various aspects of cellular shedding. They found a definite pattern of vortex shedding along the span of the cylinder and observed five distinct cells for a cylinder of 24 diameters span. Their Strouhal numbers were somewhat lower than those found by Maull and Young (1973) and attributed this due to high Reynolds number in their experiment but were fairly well in agreement with the values of Noack et al. (1991). They also compared frequencies for a sheared flow with the parallel shedding frequencies for a uniform flow at the corresponding local Reynolds number. So they modified the correlations presented by Roshko (1954) and Williamson (1988) to account for the local Reynolds number and the Strouhal number based on the centerline velocity and plotted the computed Strouhal numbers against the modified correlation given by:

$$St_w = -3.3265 / Re_{mean} + 0.1816 \times Re_{local} / Re_{mean} + 1.6 \times 10^{-4} Re_{local}^2 / Re_{mean}$$

$$St_r = 0.212 Re_{local} / Re_{mean} - 4.5 / Re_{mean}$$

The computed Strouhal numbers are less than those given by the correlations and this is attributed to the oblique nature of the shedding.

Recently, Wen and Lin (2001) investigated Strouhal-Reynolds number relationship for the two-dimensional (2-D) vortex shedding of a circular cylinder at low to medium Reynolds number using both horizontal and vertical soap film tunnels to set up a truly 2-D experiment. The St-Re curve is in good agreement with 2-D computations of Barkley and Henderson (1996). The 2-D asymptote of 0.2147 of Strouhal number is also reached. They also validated the Roshko formula for $47<Re<180$. Also they found that two separate 3-D instabilities of the natural wake at $Re \approx 180$ and 260 disappear.

CHAPTER 3

METHODOLOGY & ALGORITHM DEVELOPMENT

This chapter discusses in brief the methodology used in solving the two-dimensional Navier-Stokes equations. Solution of the Navier-Stokes equations is complicated by the lack of an independent equation for the pressure, whose gradient contributes to the two momentum equations. Pressure is a mysterious quantity in incompressible flows. It is not a thermodynamic variable as there is no "equation of state" for an incompressible fluid. It only constrains the velocity field to remain divergence-free i.e. incompressible, yet its gradient is a relevant physical quantity, force per unit area. It propagates at infinite speed in order to maintain the flow always and everywhere incompressible. One way out of this difficulty is to construct the pressure field so as to guarantee satisfaction of the continuity equation. Absolute pressure is of no significance in an incompressible flow; only the gradient of the pressure affects the flow. The momentum equations clearly determine the respective velocity components so their roles are well defined. This leaves the continuity equation, which does not contain the pressure term, to determine the pressure. So the most common method is by combining the two equations, leaving the Poisson equation for pressure which is then solved using the numerical methods.

3.1 Solution of Steady State Equations

In this section solution of the steady state i.e. time independent, Navier-Stokes equations is discussed. Finite element method is used to solve the flow problem. Galerkin weighted residual approach is used to discretize the equations. In this approach the basic equation is weighted with appropriate discrete weighing functions and the resulting equation integrated over the region of interest and equated to zero. In Galerkin approach the weighted functions are equal to the shape functions.

3.1.1 Non-Dimensionalization of Steady State Equations

The unsteady Navier-Stokes equations in two-dimensional and the continuity equation are:

$$\rho u \frac{\partial u}{\partial x} + \rho v \frac{\partial u}{\partial y} + \frac{\partial p}{\partial x} - \mu \left[\frac{\partial^2 u}{\partial x^2} + \frac{\partial^2 u}{\partial y^2} \right] = 0 \qquad \text{..... (3.1)}$$

$$\rho u \frac{\partial v}{\partial x} + \rho v \frac{\partial v}{\partial y} + \frac{\partial p}{\partial y} - \mu \left[\frac{\partial^2 v}{\partial x^2} + \frac{\partial^2 v}{\partial y^2} \right] = 0 \qquad \text{..... (3.2)}$$

$$\frac{\partial u}{\partial x} + \frac{\partial v}{\partial y} = 0 \qquad \text{..... (3.3)}$$

In dimensionless form:

$$x^* = \frac{x}{l}, y^* = \frac{y}{l}, u^* = \frac{u}{u_0}, v^* = \frac{v}{u_0} \text{ and } p^* = \frac{p}{\rho u_0^2}$$

where l is the characteristic dimension (diameter in case of a cylinder) and u_0 is the free stream velocity.

so equations (3.1), (3.2) and (3.3) become:

$$u^* \frac{\partial u^*}{\partial x^*} + v^* \frac{\partial u^*}{\partial y^*} + \frac{\partial p^*}{\partial x^*} - \frac{\mu}{\rho u_0 l} \left[\frac{\partial^2 u^*}{\partial x^{*2}} + \frac{\partial^2 u^*}{\partial y^{*2}} \right] = 0 \qquad \text{..... (3.4)}$$

$$u^* \frac{\partial v^*}{\partial x^*} + v^* \frac{\partial v^*}{\partial y^*} + \frac{\partial p^*}{\partial y^*} - \frac{\mu}{\rho u_0 l} \left[\frac{\partial^2 v^*}{\partial x^{*2}} + \frac{\partial^2 v^*}{\partial y^{*2}} \right] = 0 \qquad \text{..... (3.5)}$$

$$\frac{\partial u^*}{\partial x^*} + \frac{\partial v^*}{\partial y^*} = 0 \qquad \text{..... (3.6)}$$

Writing u in stead of u^* for convenience of presentation and $\mathrm{Re} = \frac{u_0 l \rho}{\mu}$, the Reynolds number, the equations (3.4), (3.5) and (3.6) becomes:

$$u\frac{\partial u}{\partial x}+v\frac{\partial u}{\partial y}+\frac{\partial p}{\partial x}-\frac{1}{\mathrm{Re}}\left[\frac{\partial^2 u}{\partial x^2}+\frac{\partial^2 u}{\partial y^2}\right]=0 \qquad \text{..... (3.7)}$$

$$u\frac{\partial v}{\partial x}+v\frac{\partial v}{\partial y}+\frac{\partial p}{\partial y}-\frac{1}{\mathrm{Re}}\left[\frac{\partial^2 v}{\partial x^2}+\frac{\partial^2 v}{\partial y^2}\right]=0 \qquad \text{..... (3.8)}$$

$$\frac{\partial u}{\partial x}+\frac{\partial v}{\partial y}=0 \qquad \text{..... (3.9)}$$

These are the final steady Navier-Stokes and continuity equations in the non-dinemsionalization form. Dimensionless form of Navier-Stokes equations facilities generalization to embody a large range of problems.

3.1.2 Weak form of the Governing Equations

Equations developed in the previous section are second order of differentiation. Now if the order of the governing equations is reduced, then there is need for lower order weighting functions. So weak form of the equations is formed. In weak form the order of differentiation of the governing equations is reduced.

Using the Galerkin weighted residual approach,

$$u=\sum_{i=1}^{n} N_i^u u_i \qquad \text{..... (3.10)}$$

$$v=\sum_{i=1}^{n} N_i^v v_i \qquad \text{..... (3.11)}$$

$$p=\sum_{i=1}^{n} M_i^p p_i \qquad \text{..... (3.12)}$$

where N_i^u, N_i^v and M_i^p are weight functions. Since pressure is not a thermodynamic variable, so if eight noded element is chosen, then pressure is calculated only on the four corners only. So in equations (3.10) and (3.11) n=8, while in equation (3.12) n=4.

Considering equation (3.7),

$$\int_{A^e} N_i^u \left(u\frac{\partial u}{\partial x} + v\frac{\partial u}{\partial y} + \frac{\partial p}{\partial x} - \frac{1}{\mathrm{Re}}\left[\frac{\partial^2 u}{\partial x^2} + \frac{\partial^2 u}{\partial y^2} \right] \right) dA^e = 0 \qquad \text{..... (3.13)}$$

Treating *u* as constant in $u\frac{\partial u}{\partial x}$ and v as constant in $v\frac{\partial u}{\partial y}$ and considering each term separately in the above equation:

$$\int_{A^e} N_i^u u \frac{\partial u}{\partial x} dA^e = \int_{A^e} N_i^u u^* \frac{\partial}{\partial x}\left(\sum_{j=1}^{n} N_j^u u_j \right) dA^e \qquad \text{..... (3.14)}$$

$$= \int_{A^e} N_i^u u^* \frac{\partial N_j^u}{\partial x} u_j dA^e \qquad \text{..... (3.15)}$$

Similarly,

$$\int_{A^e} N_i^u v \frac{\partial u}{\partial y} dA^e == \int_{A^e} N_i^u v^* \frac{\partial N_j^u}{\partial y} u_j dA^e \qquad \text{..... (3.16)}$$

$$\int_{A^e} N_i^u \frac{\partial p}{\partial x} dA^e == \int_{A^e} N_i^u \frac{\partial M_j^u}{\partial x} p_j dA^e \qquad \text{..... (3.17)}$$

Considering term $\int_{A^e} N_i^u \left(\frac{\partial^2 u}{\partial x^2} \right) dA^e$, applying Green's theorem, we get:

$$\int_{A^e} N_i^u \left(\frac{\partial^2 u}{\partial x^2} \right) dA^e = \int_{A^e} N_i^u \frac{\partial}{\partial x}\left(\frac{\partial u}{\partial x} \right) dA^e$$

$$= \int_{\tau} N_i^u \frac{\partial u}{\partial x}\bigg|_{\tau} d\tau - \int_{A^e} \frac{\partial N_i^u}{\partial x}\frac{\partial N_j^u}{\partial x} u_j dA^e \qquad \text{..... (3.18)}$$

Similarly,

$$\int_{A^e} N_i^u \left(\frac{\partial^2 u}{\partial y^2} \right) dA^e = \int_{\tau} N_i^u \frac{\partial u}{\partial y}\bigg|_{\tau} d\tau - \int_{A^e} \frac{\partial N_i^u}{\partial y}\frac{\partial N_j^u}{\partial y} u_j dA^e \qquad \text{..... (3.19)}$$

Now from equations (3.13), (3.15), (3.16), (3.17), (3.18) and (3.19), we get:

$$\int_{A^e} N_i^u u^* \frac{\partial N_j^u}{\partial x} u_j dA^e + \int_{A^e} N_i^u v^* \frac{\partial N_j^u}{\partial y} u_j dA^e + \int_{A^e} N_i^u \frac{\partial M_j^p}{\partial x} p_j dA^e +$$

$$\frac{1}{\mathrm{Re}}\left(\int_{A^e} \frac{\partial N_i^u}{\partial x}\frac{\partial N_j^u}{\partial x} u_j dA^e + \int_{A^e} \frac{\partial N_i^u}{\partial y}\frac{\partial N_j^u}{\partial y} u_j dA^e \right) - \frac{1}{\mathrm{Re}}\left(\int_{\tau} N_i^u \frac{\partial u}{\partial y}\bigg|_{\tau} d\tau + \int_{\tau} N_i^u \frac{\partial u}{\partial x}\bigg|_{\tau} d\tau \right) = 0$$

..... (3.20)

τ denotes the boundary of the domain

Similarly equation (3.8) and (3.9) can be written as:

$$\int_{A^e} N_i^v u^* \frac{\partial N_j^v}{\partial x} v_j dA^e + \int_{A^e} N_i^v v^* \frac{\partial N_j^v}{\partial y} v_j dA^e + \int_{A^e} N_i^v \frac{\partial M_j^p}{\partial x} p_j dA^e +$$

$$\frac{1}{\mathrm{Re}}\left(\int_{A^e} \frac{\partial N_i^v}{\partial x}\frac{\partial N_j^v}{\partial x} v_j dA^e + \int_{A^e} \frac{\partial N_i^v}{\partial y}\frac{\partial N_j^v}{\partial y} v_j dA^e \right) - \frac{1}{\mathrm{Re}}\left(\int_{\tau} N_i^v \frac{\partial v}{\partial y}\bigg|_{\tau} d\tau + \int_{\tau} N_i^v \frac{\partial v}{\partial x}\bigg|_{\tau} d\tau \right) = 0$$

..... (3.21)

$$\int_{A^e} M_i^p \frac{\partial N_j^u}{\partial x} u_j dA^e + \int_{A^e} M_i^p \frac{\partial N_j^v}{\partial v} v_j dA^e = 0 \qquad \text{…… (3.22)}$$

3.1.3 Solution of the Equations

In the previous section weak form of the governing Navier-Stokes and continuity equations are derived. In this section we will assemble the above three equations in the matrix form and develop an algorithm to solve them.

The above equations can be written in the matrix form as:

$$A\lambda = B \qquad \text{……. (3.23)}$$

where

$$\lambda_i = \begin{Bmatrix} u_i \\ v_i \\ p_i \end{Bmatrix}.$$

Each coefficient in the matrix A has the form,

$$a_{ij} = \int_{A^e} \begin{bmatrix} C_{11} & C_{12} & C_{13} \\ C_{21} & C_{22} & C_{23} \\ C_{31} & C_{32} & C_{33} \end{bmatrix} dA - \int_{\tau^e} \begin{bmatrix} \frac{1}{\mathrm{Re}} N_i^u \frac{\partial N_j}{\partial n} & 0 & 0 \\ 0 & \frac{1}{\mathrm{Re}} N_i^u \frac{\partial N_j}{\partial n} & 0 \\ 0 & 0 & 0 \end{bmatrix} dS$$

where

$$C_{11} = N_i^u u^* \frac{\partial N_j^u}{\partial x} + N_i^u v^* \frac{\partial N_j^u}{\partial y} + \frac{1}{\mathrm{Re}} \left(\frac{\partial N_i^u}{\partial x} \frac{\partial N_j^u}{\partial x} + \frac{\partial N_i^u}{\partial y} \frac{\partial N_j^u}{\partial y} \right)$$

$$C_{12} = 0 \quad , \quad C_{13} = N_i^u \frac{\partial M_j^p}{\partial x}$$

$$C_{21} = 0, \quad C_{22} = C_{11}, \quad C_{33} = N_i^v \frac{\partial M_j^p}{\partial y}$$

$$C_{31} = M_i^p \frac{\partial N_j^u}{\partial x}, \quad C_{32} = M_i^p \frac{\partial N_j^v}{\partial y}, \quad C_{33} = 0$$

Similarly, right hand side can be written as,

$$b_i = \int_{\tau} \begin{bmatrix} b_1 \\ b_2 \\ b_3 \end{bmatrix} d\tau$$

where

$$b_1 = \frac{1}{\mathrm{Re}} N_i^u \left\{ \left(\frac{\partial u_j}{\partial n} \right)^{\tau} \right\}, \; b_2 = \frac{1}{\mathrm{Re}} N_i^v \left\{ \left(\frac{\partial v_j}{\partial n} \right)^{\tau} \right\}, b_3 = 0$$

The set of non-linear simultaneous equations depicted by Eq. (3.23) are solved by a simple iterative procedure so that the results converge to a required tolerance limit. This can be summarized in the form of an algorithm as,

Step 1: Assume initial values of the primitive variables *u* and *v*.

Step 2: Form matrix A for each element and assemble it to form the global stiffness matrix.

Step 3: Solve for the updated values of *u, v* and *p.*

Step 4: Compare these new values with the previous values.

Step 5: If the results are converged to the set limits then stop else move to next step.

Step 6: Update the values of *u* and *v* and move to step 2.

3.1.4 Boundary Condition for the above Algorithm

For the above algorithm to implement in the form of a program and to solve the flow problem, for a circular cylinder which is considered in the present thesis work domain as shown in the fig. 3.1 is considered. Half of the domain is considered as the flow is symmetrical. The boundary conditions for the steady flow, referring to fig 3.1, are:

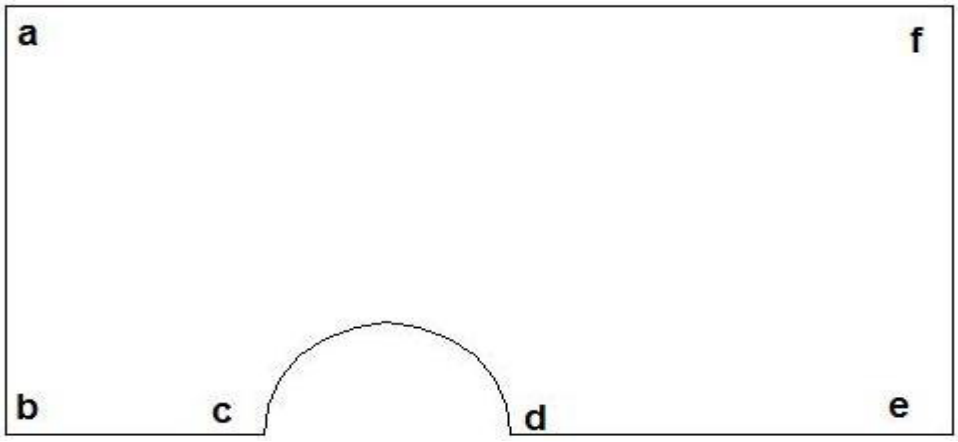

Fig 3.1 Domain for the circular cylinder problem

Boundary	Boundary Condition
ab	$u=u_0, v=0$
bc	$\partial u/\partial y = 0$

cd	u=v=0
de	$\partial u/\partial y = 0$
ef	$\partial u/\partial y = 0$
fa	$u=u_0, v=0$

3.2 Finite Difference Methods

The first step in obtaining a numerical solution is to discretize the geometric domain i.e. the numerical grid must be defined. In finite difference (FD) discretization methods the grid is usually locally structured i.e. each grid node may be considered the origin of a local coordinate system, whose axes coincide with grid lines. This implies that two grid lines belonging to the same family, say ξ_1, may not intersect, and that any pair of grid lines belonging to different families, say ξ_1= const and ξ_2 =const , intersect only once. In three dimensions, three grid lines intersect at each node and none of these intersect each other at any other point. Figure 3.2 shows examples of one-dimensional (1D) and two dimensional (2D) Cartesian grids used in finite difference methods.

Fig 3.2 an example of 1D (above) and 2D (below) Cartesian grid for FD methods

Each node is uniquely defined by a set of indices, which define the grid lines which intersect at it, (i, j) in 2D and (i, j, k) in 3D. The neighboring nodes are implicitly defined by increasing or lowering one of the indices by unity.

The equations for the given problem in the differential form, e.g. Navier-Stokes equations and continuity equation for fluid flow problem, serves as the starting point for finite difference methods. These equations are approximated by a system of linear algebraic equations, in which the variables at the grid nodes are the unknowns. The solution of this system approximates the solution to the partial differential equation.

Each node certain unknown variables associated with it and thus must provide the same number of algebraic equations. The later is a relation between the variable values at the node and at some of the neighboring nodes. It is obtained by replacing each term of the partial differential equation at the particular node by a finite difference approximation. The number of equations and unknowns must be equal. At boundary nodes where variable values are given (Dirichlet conditions), no equation is needed. When the boundary condition involve derivatives (as in Neumann conditions), the boundary condition must be discretized to provide the required equation.

3.2.1 Approximation of the First Derivative

Discretization of the partial differential equations requires the approximation of the first and higher derivatives. Here is defined the Taylor series expansion approach to approximate the first derivative.

Any continuous differentiable function $\phi(x)$ can, in the vicinity of x_i, be expressed as a Taylor series as:

$$\phi(x) = \phi(x_i) + (x - x_i)\left(\frac{\partial \phi}{\partial x}\right)_i + \frac{(x - x_i)^2}{2!}\left(\frac{\partial^2 \phi}{\partial x^2}\right)_i + \frac{(x - x_i)^3}{3!}\left(\frac{\partial^3 \phi}{\partial x^3}\right)_i + \text{.....} + \frac{(x - x_i)^n}{n!}\left(\frac{\partial^n \phi}{\partial x^n}\right)_i + H \qquad \text{……. (3.24)}$$

where H means higher order terms. By replacing x by x_{i+1} or x_{i-1} in above equation the variable values at these points in terms of the variable and its derivatives at x_i are obtained. This can be extended to any point near x_i.

Using these expansions, approximate expressions for the first and higher derivatives at point x_i in terms of the function values at neighboring points can be obtained. For example using equation (3.24) for ϕ at x_{i+1}:

$$\left(\frac{\partial \phi}{\partial x}\right)_i = \frac{\phi_{i+1} - \phi_i}{x_{i+1} - x_i} - \frac{x_{i+1} - x}{2}_i \left(\frac{\partial^2 \phi}{\partial x^2}\right)_i - \frac{\left(x_{i+1} - x_i\right)^2}{6}\left(\frac{\partial^3 \phi}{\partial x^3}\right)_i + H \quad \text{..... (3.25)}$$

Another expression can be derived using the series expansion (3.24) for ϕ at x_{i-1}:

$$\left(\frac{\partial \phi}{\partial x}\right)_i = \frac{\phi_i - \phi_{i-1}}{x_i - x_{i-1}} + \frac{x_i - x_{i-1}}{2}_i \left(\frac{\partial^2 \phi}{\partial x^2}\right)_i - \frac{\left(x_i - x_{i-1}\right)^2}{6}\left(\frac{\partial^3 \phi}{\partial x^3}\right)_i + H \quad \text{..... (3.26)}$$

Still another expression can be obtained by using equation (3.24) at both x_{i-1} and x_{i+1}:

$$\left(\frac{\partial \phi}{\partial x}\right)_i = \frac{\phi_{i+1} - \phi_{i-1}}{x_{i+1} - x_{i-1}} - \frac{(x_{i+1} - x_i)^2 - (x_i - x_{i-1})^2}{2\left(x_{i+1} - x_{i-1}\right)}\left(\frac{\partial^2 \phi}{\partial x^2}\right)_i -$$

$$\frac{(x_{i+1} - x_i)^3 - (x_i - x_{i-1})^3}{6\left(x_{i+1} - x_{i-1}\right)} \left(\frac{\partial^3 \phi}{\partial x^3}\right)_i + H \quad \text{..... (3.27)}$$

All the three expressions obtained above are exact if all the terms on the right hand side are retained. However, if the distance between the grid points, i.e. $x_i - x_{i-1}$ and $x_{i+1} - x_i$ is small, the higher order terms will be small except in unusual situation in which the higher derivatives are locally very large. Ignoring the later possibility, the approximations of the first derivative result from truncating terms on the right hand side after the first term in the above series:

$$\left(\frac{\partial \phi}{\partial x}\right)_i \approx \frac{\phi_{i+1} - \phi_i}{x_{i+1} - x_i} \quad \text{..... (3.28)}$$

$$\left(\frac{\partial \phi}{\partial x}\right)_i \approx \frac{\phi_i - \phi_{i-1}}{x_i - x_{i-1}} \qquad \text{..... (3.29)}$$

$$\left(\frac{\partial \phi}{\partial x}\right)_i \approx \frac{\phi_{i+1} - \phi_{i-1}}{x_{i+1} - x_{i-1}} \qquad \text{..... (3.30)}$$

These are called forward difference (FDS), backward difference (BDS) and central (CDS) difference schemes respectively. The terms that are deleted from the right hand side are called the truncation errors and they measure the accuracy of the approximation and determine the rate at which the error decreases as the spacing between the points is reduced. Higher order approximations of the first derivative can be obtained by using more points to eliminate more of the truncation error terms in the above expressions.

3.2.2 Approximation of the Second Derivative

The CDS approach is used and it requires the first derivative at x_{i-1} and x_{i+1}. But better choice is to evaluate $\frac{\partial \phi}{\partial x}$ at points halfway between x_i and x_{i+1} and x_i and x_{i-1}. The CDS approximations for these first derivatives, respectively, are:

$$\left(\frac{\partial \phi}{\partial x}\right)_{i+\frac{1}{2}} \approx \frac{\phi_{i+1} - \phi_i}{x_{i+1} - x_i} \quad \text{and} \quad \left(\frac{\partial \phi}{\partial x}\right)_{i-\frac{1}{2}} \approx \frac{\phi_i - \phi_{i-1}}{x_i - x_{i-1}}$$

The resulting expression for the second derivative is:

$$\left(\frac{\partial^2 \phi}{\partial x^2}\right)_i \approx \frac{\left(\frac{\partial \phi}{\partial x}\right)_{i+\frac{1}{2}} - \left(\frac{\partial \phi}{\partial x}\right)_{i-\frac{1}{2}}}{\frac{1}{2}\left(x_{i+1} - x_{i-1}\right)} \approx$$

$$\frac{\phi_{i+1}\left(x_i - x_{i-1}\right) + \phi_{i-1}\left(x_{i+1} - x_i\right) - \phi_i\left(x_{i+1} - x_{i-1}\right)}{\frac{1}{2}\left(x_{i+1} - x_{i-1}\right)\left(x_{i+1} - x_i\right)\left(x_i - x_{i-1}\right)} \qquad \text{..... (3.31)}$$

For equidistant spacing of the points, expression (3.31) becomes:

$$\left(\frac{\partial^2 \phi}{\partial x^2}\right)_i \approx \frac{\phi_{i+1} + \phi_{i-1} - 2\phi_i}{(\Delta x)^2} \qquad \text{..... (3.32)}$$

The approximation is second order accurate when the spacing between the points is uniform. Even when the grid is non-uniform the truncation error is reduced when the grid is refined. Higher order approximations can be obtained by using more data points i.e. x_{i-2} and x_{i+2}.

3.2.3 Implementation of Boundary Conditions

A FD approximation of a partial differential equation is required at every interior grid point. To render the solution unique, the continuous problem requires information about the solution at the domain boundaries. Generally, the value of the variable at the boundary (Dirichlet type boundary condition) or its gradient in a particular direction (usually normal to the boundary, Neumann boundary conditions) or a linear combination of the two quantities is given.

If the variable value is known at some boundary point, then there is no need to solve for it. In all FD equations which contain data at these points, the known value is used and nothing further is necessary. A problem does arise when higher order approximations of the derivatives are used, since they require data at more than three points, approximations at interior nodes may demand data at points beyond the boundary. It may then be necessary to use differential approximations for the derivatives at the points close to boundary; usually these arte of lower order than the approximations used deeper in the interior and may be one sided differentiations. The accuracy of the results depends not only on the approximation used, but also on the accuracy of the values at the interior nodes.

3.2.4 Errors in Finite Difference Methods

As discussed above in the solution of differential equations with finite differences, a variety of schemes are available for the discretization of derivatives and solution of the resulting system of the algebraic equations. There are a

number of errors involved in the numerical computations. Some of these are discussed below:

Round-off errors: Computations are rarely made in exact arithmetic. This means that real numbers are represented in "floating point" form and as a result errors are caused due to the rounding off the real numbers. Even though modern computers can represent number to 12 or more places of decimal, in extreme cases such errors, called "round off" errors, can accumulate and become a main source of error.

Truncation Error: In finite difference representation of derivatives with Taylor's series expansion, the higher order terms are neglected by truncating the series and the error caused as a result of such truncation is called truncation error.

The truncation error identifies the difference between the exact solution of a differential equation and its finite difference solution without the round off error, i.e.

$$\begin{pmatrix} Exact\ \ solution \\ of\quad PDE \end{pmatrix} - \begin{pmatrix} Solution\ \ of\ \ finite \\ difference\ \ equation \\ without\ \ the \\ round-off\ \ error \end{pmatrix} = \begin{pmatrix} Truncation \\ error \end{pmatrix}$$

The terminology discretization error is used to identify the error involved due to the truncation error in the finite difference representation of governing differential equations and boundary conditions.

Consistency: One of the requirements of finite difference approximation is that in the limiting process as the step size (i.e., $\Delta x, \Delta t$ etc.) becomes extremely small the finite difference approximation should become arbitrarily close to the derivatives. This requirement implies that the truncation error should vanish as the step size vanishes. Then the finite difference approximation is said to be consistent with the original differential equation.

Stability: In numerical solution of differential equations with finite differences, errors are introduced at almost every stage of the calculations. The solution scheme is said to be stable if the error involved in numerical computations are not amplified without bounds as the numerical calculations progresses.

Convergence: The numerical solution is said to be convergent, if the numerical solution approaches the exact solution of the problem as the time and space steps tend to zero. It is to be noted that the conditions of stability, consistency and convergence are related to each other.

The total error involved in finite difference calculations consists of the discretization error plus the round off error. The discretization error increases with increasing mesh size while the round-off error decreases with increasing mesh size. Therefore, the total error is expected to exhibit a minimum as the mesh size is decreased.

3.3 Schemes for Solving Unsteady Navier-Stokes equations

In this section some of the most common methods used for solving the Navier-Stokes equations are discussed. The methods discussed are explicit time advance scheme, implicit time advance scheme and fractional step method

3.3.1 Simple Explicit Time Advance Scheme

When the velocity field at the $(n+1)^{th}$ time step is obtained from the velocity field at the n^{th} time step the method is called explicit time advancing scheme. Using this method the Poisson equation for the pressure is constructed and it plays the role of enforcing the continuity. The procedure is briefly explained below.

The momentum or Navier-Stokes equations can be written symbolically as:

$$\frac{\partial(\rho u_i)}{\partial t} = -\frac{\delta(\rho u_i u_j)}{\partial x_j} - \frac{\delta p}{\delta x_i} + \frac{\delta \tau_{ij}}{\delta x_j} \qquad \text{..... (3.33)}$$

where $\tau_{ij} = \mu\left(\frac{\partial u_i}{\partial x_j} + \frac{\partial u_j}{\partial x_i}\right) - \frac{2}{3}\mu\delta_{ij}\frac{\partial u_j}{\partial x_i}$

or $$\frac{\partial(\rho u_i)}{\partial t} = H_i - \frac{\delta p}{\delta x_i} \qquad \text{..... (3.34)}$$

Where $\partial/\partial x$ represents a discretized spatial derivative (which could represent a different approximation in each term) and H_i is shorthand notation for the advective and viscous terms.

Now solving Eq. (3.34) with the explicit Euler method for time advancement we have

$$(\rho u_i)^{n+1} - (\rho u_i)^n = \Delta t\left(H_i^n - \frac{\delta p^n}{\delta x_i} \right) \qquad \text{..... (3.35)}$$

To apply this method the velocity at time step *n* is used to compute H_i^n and, if the pressure is available $\delta p^n / \delta x_i$ may also be computed. This give an estimation of ρu_i at new time step *n+1* but the velocity field does not satisfy the continuity equation.

$$\frac{\delta (\rho u_i)^{n+1}}{\delta x_i} = 0 \qquad \text{..... (3.36)}$$

Now to enforce the continuity, let us take the numerical divergence (using the numerical operator used to approximate the continuity equation) of equation (3.38). This gives:

$$\frac{\delta(\rho u_i)^{n+1}}{\delta x_i} - \frac{\delta(\rho u_i)^n}{\delta x_i} = \Delta t\left[\frac{\delta}{\delta x_i}\left(H_i^n - \frac{\delta p^n}{\delta x_i} \right) \right] \qquad \text{..... (3.37)}$$

Now the first term is divergence of the new velocity field which we want to be zero. The second term is zero if the continuity is enforced at time step n; if continuity equation is enforced this term should be zero else this term is left in the equation. Retaining this term is necessary when an iterative method is used to solve the Poisson equation for the pressure and the iterative process is not completely converged. Now taking all this into account, the result is the discrete Poisson equation for pressure p^n.

$$\frac{\delta}{\delta x_i}\left(\frac{\delta p^n}{\delta x_i}\right) = \frac{\delta H_i^n}{\delta x_i} \qquad \text{..... (3.38)}$$

The operator $\partial/\partial x$ outside the parenthesis is the divergence operator inherited from the continuity equation, while $\delta p / \delta x_i$ is pressure gradient from the momentum equations. If the pressure p^n satisfy this discrete Poisson equation, the velocity field at time step *n+1* will divergence free. It should be noted that the time step to which the pressure belongs is arbitrary.

This provides the following algorithm for time advancing the Navier-Stroke equations:

- Start with a velocity field u at time t^n.
- Compute the combination, H_i^n of the advective and viscous term and its divergence (both need to be retained for later use).
- Solve the Poisson equation for the pressure p^n.
- Compute the velocity field at new time step.
- Now stage is set for the new time step.

3.3.2 Implicit Time Advancing Scheme

In this method all the terms are evaluated in terms of the unknown variable values at the new time level. The Poisson equation for the pressure is constructed and it plays the role of enforcing the continuity. The procedure is briefly explained below.

Solving Eq. 3.33 using the implicit time advancing scheme, we get:

$$\left(\rho u_i\right)^{n+1} - \left(\rho u_i\right)^n = \Delta t\left(\frac{\delta\left(\rho u_i u_j\right)^{n+1}}{\delta x_j} - \frac{\delta p^{n+1}}{\delta x_i} + \frac{\delta \tau_{ij}^{n+1}}{\delta x_j}\right) \qquad \text{..... (3.39)}$$

Now there are a number of difficulties that were not present in the explicit method. First, there is a problem with the pressure. The divergence of the velocity at the new time step must be zero. This can be accomplished in much the same way as in the explicit method. Taking divergence of the Eq. (3.39),

assuming that velocity at the time step *n* is divergence free (this can be corrected if necessary) and at the new time step *n+1* also. So this leads to the Poisson equation for the pressure:

$$\frac{\delta}{\delta x_i}\left(\frac{\delta\left(\rho u_i\right)^{n+1}}{\delta x_i}\right)=\frac{\delta}{\delta x_i}\left(\frac{\delta\left(\rho u_i u_j\right)^{n+1}}{\delta x_j}\right) \qquad \text{..... (3.40)}$$

Now the term on the right hand side cannot be computed until the computations of the velocity field at the time *n+1* is computed and vice versa. So the Poisson equation and the momentum equations have to be solved simultaneously. This can be done only with an iterative method.

Next, even if the pressures were known, Eqs. (3.40) are a large system of non-linear equations which must be solved for the velocity field. The structure of this system of equations is essentially the same as the structure of the matrix of the finite differenced Laplace equation so solving them is far from a trivial matter. If one wishes to solve them accurately, the best procedure is to adopt the converged results from the preceding time step as the initial guess for the new velocity field and then converge to the solution at the new time step using the Newton-Raphson iteration method or a secant method designed for systems.

An alternative way of dealing with the non-linearity is linearizing the equations about the result at the preceding time step. If we write:

$$u_i^{n+1}=u_i^n+\Delta u_i \qquad \text{..... (3.41)}$$

Then the non-linear terms in Eqs. (3.40) can be expressed as:

$$u_i^{n+1}u_j^{n+1}=u_i^n u_j^n+u_i^n\Delta u_j+u_j^n\Delta u_i+\Delta u_i\Delta u_j \qquad \text{..... (3.42)}$$

For small value of Δt, $\Delta u_i \approx \Delta t\ \partial u_i/\partial t$, so the last term in the above equation is of second order in Δt and is smaller in magnitude than the error made in the discretization. It can be therefore be neglected.

Now the Eq. (3.40) can be written as:

$$\rho\ \Delta u_i=\Delta t\left(\frac{\delta\left(\rho u_i u_j\right)^n}{\delta x_j}+\frac{\delta\left(\rho u_i^n\Delta u_j\right)}{\delta x_j}+\frac{\delta\left(\rho\Delta u_i u_j^n\right)}{\delta x_j}-\frac{\delta p^n}{\delta x_i}-\right.$$

$$\frac{\delta \Delta p}{\delta x_i} + \frac{\delta \tau_{ij}^{n}}{\delta x_j} + \frac{\delta \Delta \tau_{ij}}{\delta x_j} \Bigg) \qquad \text{..... (3.43)}$$

This method takes advantage of the fact that the non-linearity is quadratic and removes most of the difficulties arising from it. However, still a large system of linear equations needs to be solved with the above structure. Direct solution of such a system is too expensive and so the solution is found iteratively. Implicit methods allow large time steps to be used without instability, so they often are used to solve the steady state problems.

3.3.3 Fractional step Method

The fractional step concept is more a generic approach than a particular method. It is an approximate factorization of a method; let us take the explicit advancement of the Navier-Stokes equations in symbolic form:

$$u_i^{n+1} = u_i^n + (C_i + D_i + P_i)\,\Delta t \qquad \text{..... (3.44)}$$

where C_i, D_i, and P_i represent the convective, diffusive and pressure terms, respectively. The equation can be split into a three step method:

$$u_i^{*} = u_i^n + (C_i)\,\Delta t \qquad \text{..... (3.45)}$$

$$u_i^{**} = u_i^{*} + (D_i)\,\Delta t \qquad \text{..... (3.46)}$$

$$u_i^{n+1} = u_i^{**} + (P_i)\,\Delta t \qquad \text{..... (3.47)}$$

In the third step, P_i is the gradient of the quantity that obeys the Poisson equation; so this quantity must be chosen so that the continuity equation is satisfied. Depending upon the particulars of the method the source term in this Poisson equation may different slightly from the source term in the standard Poisson equation for the pressure (3.38). For this reason, the variable is called the pseudo-pressure or a pressure like variable. Also, it is possible to split the convective and diffusive terms further; for example, they may be split into their components in their various coordinate directions. Clearly, many basic methods can be used and many kinds of splitting can be applied to each.

From the methods discussed above, use of the implicit method allows arbitrarily large time steps to be taken. This property is useful in studying the flow with slow transients or steady flows. When implicit method is used with central difference scheme on coarse grids oscillatory solutions are produced but the scheme remains stable. Also in this method there is first order truncation error in time and there are a large number of equations to be solved at each time step. Also implicit methods require much more storage than the explicit schemes. If the time step is large, the fractional step method produces an error due to the operator splitting. This error can be eliminated by reducing the time step. If the splitting error is significant, the discretization error is also large. So explicit time marching scheme is used in the work presented here as in explicit scheme time steps can be taken small and it gives a complete history of the flow.

3.4 Solution of Unsteady Equations

Based on the explicit time advancing scheme, here an algorithm is developed to solve the unsteady two dimensional Navier-Stokes equations and the continuity equation. The equations are used in the Cartesian form.

3.4.1 Non-Dimensionalization of the Unsteady Equations

The unsteady Navier-Stokes equations in two-dimensional and the continuity equation are:

$$\rho \frac{\partial u}{\partial t} + \rho u \frac{\partial u}{\partial x} + \rho v \frac{\partial u}{\partial y} + \frac{\partial p}{\partial x} - \mu \left[\frac{\partial^2 u}{\partial x^2} + \frac{\partial^2 u}{\partial y^2} \right] = 0 \qquad \text{..... (3.48)}$$

$$\rho \frac{\partial v}{\partial t} + \rho u \frac{\partial v}{\partial x} + \rho v \frac{\partial v}{\partial y} + \frac{\partial p}{\partial y} - \mu \left[\frac{\partial^2 v}{\partial x^2} + \frac{\partial^2 v}{\partial y^2} \right] = 0 \qquad \text{..... (3.49)}$$

$$\frac{\partial u}{\partial x} + \frac{\partial v}{\partial y} = 0 \qquad \text{..... (3.50)}$$

In dimensionless form:

$$x^* = \frac{x}{l}, y^* = \frac{y}{l}, u^* = \frac{u}{u_0}, v^* = \frac{v}{u_0} \text{ and } p^* = \frac{p}{\rho u_0^2}$$

where l is the characteristic (diameter in case of a cylinder) and

u_0 is the free stream velocity.

So equations (3.48), (3.49) and (3.50) become:

$$\frac{\partial u^*}{\partial t} + u^* \frac{\partial u^*}{\partial x^*} + v^* \frac{\partial u^*}{\partial y^*} + \frac{\partial p^*}{\partial x^*} - \frac{\mu}{\rho u_0 l}\left[\frac{\partial^2 u^*}{\partial x^{*2}} + \frac{\partial^2 u^*}{\partial y^{*2}}\right] = 0$$

$$\frac{\partial v^*}{\partial t} + u^* \frac{\partial v^*}{\partial x^*} + v^* \frac{\partial v^*}{\partial y^*} + \frac{\partial p^*}{\partial y^*} - \frac{\mu}{\rho u_0 l}\left[\frac{\partial^2 v^*}{\partial x^{*2}} + \frac{\partial^2 v^*}{\partial y^{*2}}\right] = 0$$

$$\frac{\partial u^*}{\partial x^*} + \frac{\partial v^*}{\partial y^*} = 0$$

Writing u in stead of u^* for convenience of presentation and $\text{Re} = \frac{u_0 l \rho}{\mu}$, the Reynolds number, the above equations becomes:

$$\frac{\partial u}{\partial t} + u \frac{\partial u}{\partial x} + v \frac{\partial u}{\partial y} + \frac{\partial p}{\partial x} - \frac{1}{\text{Re}}\left[\frac{\partial^2 u}{\partial x^2} + \frac{\partial^2 u}{\partial y^2}\right] = 0 \quad \text{..... (3.51)}$$

$$\frac{\partial v}{\partial t} + u \frac{\partial v}{\partial x} + v \frac{\partial v}{\partial y} + \frac{\partial p}{\partial y} - \frac{1}{\text{Re}}\left[\frac{\partial^2 v}{\partial x^2} + \frac{\partial^2 v}{\partial y^2}\right] = 0 \quad \text{..... (3.52)}$$

$$\frac{\partial u}{\partial x} + \frac{\partial v}{\partial y} = 0 \quad \text{..... (3.53)}$$

These are the final Navier-Stokes and continuity equations in the non-dinemsionalization form. The advantage of the non-dimensional equations is that one can find the flow pattern at various Reynolds number by only changing the free stream velocity and the other parameters remaining constant. In the next section these equations will be considered for the further developments of the algorithm.

3.4.2 Development of Poisson Equation

In this section, explicit time advancing algorithm is used to develop the Poisson equation for the calculation of the pressure terms. Non-dimensional equations developed in the previous section are used to develop the equation. As there is no equation of state for the pressure terms so the above equations will be combined to form the equations. The procedure is described below:

Equations (3.51) and (3.52) can be written as:

$$\frac{\partial u}{\partial t} = \frac{1}{\mathrm{Re}}\left[\frac{\partial^2 u}{\partial x^2} + \frac{\partial^2 u}{\partial y^2}\right] - u\frac{\partial u}{\partial x} - v\frac{\partial u}{\partial y} - \frac{\partial p}{\partial x}$$

$$\frac{\partial v}{\partial t} = \frac{1}{\mathrm{Re}}\left[\frac{\partial^2 v}{\partial x^2} + \frac{\partial^2 v}{\partial y^2}\right] - u\frac{\partial v}{\partial x} - v\frac{\partial v}{\partial y} - \frac{\partial p}{\partial y}$$

or

$$\frac{\partial u}{\partial t} = H_1 - \frac{\partial p}{\partial x} \qquad \text{..... (3.54)}$$

$$\frac{\partial v}{\partial t} = H_2 - \frac{\partial p}{\partial y} \qquad \text{..... (3.55)}$$

where *H* denotes the sum of advective and viscous terms.

Now solving equations (3.54) and (3.55) by the explicit time advancing scheme, we get:

$$u^{n+1} - u^n = \Delta t\left(H_1^n - \frac{\partial p^n}{\partial x}\right) \qquad \text{..... (3.56)}$$

$$v^{n+1} - v^n = \Delta t\left(H_2^n - \frac{\partial p^n}{\partial y}\right) \qquad \text{..... (3.57)}$$

The above equations must also satisfy the continuity equation at all the time steps. The continuity at the time step *n+1* is given by:

$$\frac{\partial u^{n+1}}{\partial x} + \frac{\partial v^{n+1}}{\partial y} = 0 \qquad \text{..... (3.58)}$$

Now to enforce the continuity equation, taking the numerical divergence of the Eqs. (3.56) and (3.57) using the same numerical operators used to approximate the continuity equation, we get:

$$\frac{\partial u^{n+1}}{\partial x} - \frac{\partial u^{n}}{\partial x} = \Delta t \left(\frac{\partial H_1^{n}}{\partial x} - \frac{\partial}{\partial x}\left(\frac{\partial p^{n}}{\partial x} \right) \right)$$

$$\frac{\partial v^{n+1}}{\partial y} - \frac{\partial v^{n}}{\partial y} = \Delta t \left(\frac{\partial H_2^{n}}{\partial y} - \frac{\partial}{\partial y}\left(\frac{\partial p^{n}}{\partial y} \right) \right)$$

Adding the above two terms and forcing the continuity equation (3.58)

$$-\frac{\partial u^{n}}{\partial x} - \frac{\partial v^{n}}{\partial y} = \Delta t \left(\frac{\partial H_1^{n}}{\partial x} + \frac{\partial H_2^{n}}{\partial y} - \frac{\partial}{\partial x}\left(\frac{\partial p^{n}}{\partial x} \right) - \frac{\partial}{\partial y}\left(\frac{\partial p^{n}}{\partial y} \right) \right)$$

or

$$\frac{\partial}{\partial x}\left(\frac{\partial p^{n}}{\partial x} \right) + \frac{\partial}{\partial y}\left(\frac{\partial p^{n}}{\partial y} \right) = \frac{\partial H_1^{n}}{\partial x} + \frac{\partial H_2^{n}}{\partial y} + \frac{1}{\Delta t}\left(\frac{\partial u^{n}}{\partial x} + \frac{\partial v^{n}}{\partial y} \right) \qquad \text{..... (3.59)}$$

This is the Poisson equation which is used to calculate the pressure at the n^{th} time step. The third term on the right, $\frac{\partial u^{n}}{\partial x} + \frac{\partial v^{n}}{\partial y}$, is zero if the continuity is enforced at the n^{th} time step. If this is not the case this term should be retained in the equation. Assuming that the continuity is enforced at the n^{th} time step, the final Poisson equation becomes:

$$\frac{\partial}{\partial x}\left(\frac{\partial p^{n}}{\partial x} \right) + \frac{\partial}{\partial y}\left(\frac{\partial p^{n}}{\partial y} \right) = \frac{\partial H_1^{n}}{\partial x} + \frac{\partial H_2^{n}}{\partial y} \qquad \text{..... (3.60)}$$

3.4.3 Discretization of Equations

In this section the Poisson equation obtained in the previous section is discretized using the finite difference methods. It is should be noted that the Laplacian operator in the pressure equation is the product of the divergence operator originating from the continuity equation and the gradient operator that

comes from the momentum equations. In a numerical approximation, it is essential that the consistency of these operators be maintained i.e. the approximation of the Poisson's equations must be defined as the product of divergence and gradient approximations used in the basic equations. Violation of this constraint leads to lack of satisfaction of the continuity equation. To emphasize the importance of this issue, the two derivatives of the pressure in the above equations are separated: the outer derivative stems from the continuity equation while the inner derivative arises from the momentum equations. The outer and inner derivatives may be discretized using different schemes-they have to be those used in the momentum and continuity equations.

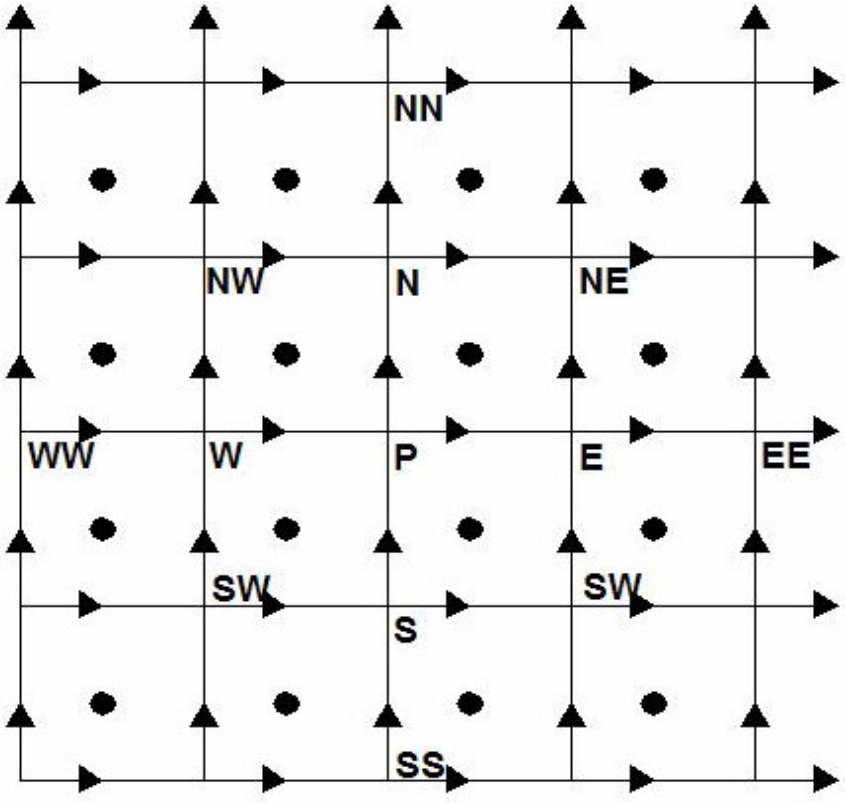

Fig 3.3 Arrangement of velocity components and pressure on a FD grid

Grid arrangement chosen to store the variable is shown in fig 3.3. Pressure is calculated at the centre of the cell whereas velocities are calculated and stored at the grid points. Arrows denotes the velocity and dots denote the pressure.

So referring to the above arrangement of storage of variables and using the forward difference scheme for Navier-Stokes equations and backward difference scheme for the continuity equation, discretizing equation (3.60) we get:

$$\frac{\partial}{\partial x}\left(\frac{\partial p^n}{\partial x}\right)+\frac{\partial}{\partial y}\left(\frac{\partial p^n}{\partial y}\right)=\frac{\left(\frac{\partial p^n}{\partial x}\right)_P-\left(\frac{\partial p^n}{\partial x}\right)_W}{\Delta x}+\frac{\left(\frac{\partial p^n}{\partial y}\right)_P-\left(\frac{\partial p^n}{\partial y}\right)_S}{\Delta y}$$

$$=\frac{\frac{p_E^n-p_P^n}{\Delta x}-\frac{p_P^n-p_W^n}{\Delta x}}{\Delta x}+\frac{\frac{p_N^n-p_P^n}{\Delta y}-\frac{p_P^n-p_S^n}{\Delta y}}{\Delta y}$$

$$=p_P^n\left(-\frac{2}{(\Delta x)^2}-\frac{2}{(\Delta y)^2}\right)+\frac{p_E^n}{(\Delta x)^2}+\frac{p_W^n}{(\Delta x)^2}+\frac{p_N^n}{(\Delta y)^2}+\frac{p_S^n}{(\Delta y)^2}$$

…….. (3.61)

where Δx is the spacing in the x-direction and Δy is the spacing in the y-direction, assuming uniform spacing in both the directions. P is the point at which the discretization is done and E, W, S, N denotes grid point in the east, west, south and north directions of the point P.

$$\frac{\partial H_1^n}{\partial x}+\frac{\partial H_2^n}{\partial y}=\frac{H_{1,P}^n-H_{1,W}^n}{\Delta x}+\frac{H_{2,P}^n-H_{2,S}^n}{\Delta y} \qquad \text{…….. (3.62)}$$

If the continuity is not forced at the n^{th} time step then third equation on the right hand side of equation (3.59) needs to be retained. So, discretizing of the third term gives:

$$\frac{\partial u^n}{\partial x}+\frac{\partial v^n}{\partial y}=\frac{u_P^n-u_W^n}{\Delta x}-\frac{u_P^n-u_S^n}{\Delta y} \qquad \text{……. (3.63)}$$

From Eqs. (3.60), (3.61) and (3.62)

$$p_P^n\left(-\frac{2}{(\Delta x)^2}-\frac{2}{(\Delta y)^2}\right)+\frac{p_E^n}{(\Delta x)^2}+\frac{p_W^n}{(\Delta x)^2}+\frac{p_N^n}{(\Delta y)^2}+\frac{p_S^n}{(\Delta y)^2}=\frac{H_{1,P}^n-H_{1,W}^n}{\Delta x}+\frac{H_{2,P}^n-H_{2,S}^n}{\Delta y}$$

or

$$p_P^n = \frac{\dfrac{H_{1,P}^n - H_{1,W}^n}{\Delta x} + \dfrac{H_{2,P}^n - H_{2,S}^n}{\Delta y} - \left(\dfrac{p_E^n}{(\Delta x)^2} + \dfrac{p_W^n}{(\Delta x)^2} + \dfrac{p_N^n}{(\Delta y)^2} + \dfrac{p_S^n}{(\Delta y)^2} \right)}{\left(-\dfrac{2}{(\Delta x)^2} - \dfrac{2}{(\Delta y)^2} \right)} \quad \text{..... (3.64)}$$

There is also need for some treatment of *H*; sum of advective and viscous terms, to find is values at the grid points.

$$H_1 = \frac{1}{\mathrm{Re}} \left(\frac{\partial^2 u}{\partial x^2} + \frac{\partial^2 u}{\partial y^2} \right) - u \frac{\partial u}{\partial x} - v \frac{\partial u}{\partial y}$$

$$H_2 = \frac{1}{\mathrm{Re}} \left(\frac{\partial^2 v}{\partial x^2} + \frac{\partial^2 v}{\partial y^2} \right) - u \frac{\partial v}{\partial x} - v \frac{\partial v}{\partial y}$$

Discretizing above equations using central difference for second derivatives and backward difference for first derivatives, we get:

$$H_1^n = \frac{1}{\mathrm{Re}} \left(\frac{\left(\dfrac{\partial u}{\partial x} \right)_P^n - \left(\dfrac{\partial u}{\partial x} \right)_W^n}{\Delta x} + \frac{\left(\dfrac{\partial u}{\partial y} \right)_P^n - \left(\dfrac{\partial u}{\partial y} \right)_S^n}{\Delta y} \right) -$$

$$\left(u_P^n \left(\frac{u_P^n - u_W^n}{\Delta x} \right) + v_P^n \left(\frac{u_P^n - u_S^n}{\Delta y} \right) \right)$$

or

$$= \frac{1}{\mathrm{Re}} \left(\frac{\dfrac{u_E^n - u_P^n}{\Delta x} - \dfrac{u_P^n - u_W^n}{\Delta x}}{\Delta x} + \frac{\dfrac{u_N^n - u_P^n}{\Delta y} - \dfrac{u_P^n - u_S^n}{\Delta y}}{\Delta y} \right) -$$

$$\left(u_P^n \left(\frac{u_P^n - u_W^n}{\Delta x} \right) + v_P^n \left(\frac{u_P^n - u_S^n}{\Delta y} \right) \right)$$

or

$$H_1^n = \frac{1}{\mathrm{Re}}\left(\frac{u_E^n - 2*u_P^n + u_W^n}{(\Delta x)^2} + \frac{u_N^n - 2*u_P^n + u_S^n}{(\Delta y)^2}\right) - \left(u_P^n\left(\frac{u_P^n - u_W^n}{\Delta x}\right) + v_P^n\left(\frac{u_P^n - u_S^n}{\Delta y}\right)\right)$$

..... (3.65)

Similarly,

$$H_2^n = \frac{1}{\mathrm{Re}}\left(\frac{v_E^n - 2*v_P^n + v_W^n}{(\Delta x)^2} + \frac{v_N^n - 2*v_P^n + v_S^n}{(\Delta y)^2}\right) - \left(u_P^n\left(\frac{v_P^n - v_W^n}{\Delta x}\right) + v_P^n\left(\frac{v_P^n - v_S^n}{\Delta y}\right)\right)$$

..... (3.66)

These values of *H* are stored and are used in the solution of the equations for velocities at the next tine step.

3.4.4 Solution of the Equations

In this section procedure is defined to solve for pressure and velocities. First, using the Eq. (3.66) pressure is calculated at the center of all the cells. If the continuity is not forced at the n^{th} time step then equation (3.65) is also added to this equation's right hand side. Now from Eqs (3.58) and (3.59)

$$u^{n+1} = u^n + \Delta t\left(H_1^n - \frac{\partial p^n}{\partial x}\right) \quad \text{..... (3.67)}$$

$$v^{n+1} = v^n + \Delta t\left(H_2^n - \frac{\partial p^n}{\partial y}\right) \quad \text{..... (3.68)}$$

After this above equations are used to calculate the velocity at the next time step. Values of u^n, v^n, H_1^n, H_2^n are known at the n^{th} time step and only derivatives of pressure are not known. These can be found by using one of the finite difference schemes using the newly calculated pressure terms and hence values of the velocities of the new time step are calculated.

Using these newly found velocities pressure at the next time step is calculated and then pressure is used to calculate the velocities at the next time step and the process goes on. So following the above described procedure following algorithm can be developed:

Step 1: Start with the velocity field u_i^n and v_i^n at time t^n as initial guess.

Step 2: Compute the combination, $H_1^n and\ H_2^n$ of the advective and viscous term.

Step 3: Calculate the pressure using discretized Poisson equation.

Step 4: Compare the pressure with the old pressure values at same time step.

Step 5: If the pressure is converged to the set limits, move to step 6 else move to step 3.

Step 6: Using this pressure field calculate the values of the velocities at the next time step using the Navier-Stokes equations.

Step 7: Now stage is set for the next time step. Use these values of velocities as the initial guess for the next time step and move to step 2.

3.4.5 Boundary Condition for the above Algorithm

For the above algorithm to implement in the form of a program and to solve the flow problem, for a circular cylinder which is considered in the present thesis work domain as shown in the fig. 3.1 is considered. Half of the domain is considered as the flow is symmetrical. The boundary conditions for the unsteady flow, referring to fig 3.1, are:

Boundary	Boundary Condition
ab	$u=u_0$, $v=0$
bc	$v=0$
cd	$u=v=0$
de	$v=0$
ef	$u=u_0$, $v=0$
fa	$u=u_0$, $v=0$

CHAPTER 4

COMPUTER IMPLEMETATION

To prove the validity of the algorithms developed in the previous section, programs were made in Turbo C++ on a DOS platform which implemented these algorithms; this section discusses the programming details. The program is divided into various functions which are discussed briefly below:

4.1 Computer Implementation of steady state problem

Here functions of the program developed to study steady state problem are discussed.

4.1.1 main()

This function is the point from where program execution starts. It calls the following functions in the order mentioned; details of these functions are given in following sections:

- read_data()
- bandWidth()
- bc_and_coding()
- alocMem()
- ele_stiff_matrix()
- assemble()
- solve()
- iterate()

4.1.2 read_data()

This function reads the data such as no of nodes, elements, element connectivity of the elements, and the coordinates of each node from a data file.

4.1.3 bandWidth()

This function calculates the band width of the element stiff matrix to store the coefficients of matrix A. this function calls the following function in itself,

- form_eqn()

4.14 form_eqn()

This function calculates and stores the degree of freedom of each node.

4.1.5 bc_and_coding()

This function adds the boundary conditions to the values prescribed at different nodes. It also codes the elements which are on the boundary.

4.1.6 alocMem()

This function allocates memory to the global element stiffness matrix.

4.1.7 ele_stiff_matrix()

This function calculates the coefficients of the element stiffness matrix A and also of matrix B. it calls in itself a number of functions to calculate the coefficients. These in the order of call are,

- shape_8()
- shape_4()
- J_matrix_N()
- J_matrix_M()
- Value_matrix()

4.1.8 shape_8()

This function calculates the shape functions and local derivatives of the shape functions for the eight noded elements.

4.1.9 shape_4()

This function calculates the shape functions and local derivatives of the shape functions for the four noded elements.

4.1.10 J_matrix_N()

This function calculates the jacobian matrix, inverse of the jacobian matrix and the global derivatives of the shape functions for the eight noded elements.

4.1.11 J_matrix_M()

This function calculates the jacobian matrix, inverse of the jacobian matrix and the global derivatives of the shape functions for the four noded elements.

4.1.12 value_matrix()

This matrix calculates the value of the B matrix on the boundaries of the elements on which the velocity values are prescribed. This function in itself calls following function in the order mentioned below,

- side_1()
- side_2()
- side_3()
- side_4()

These functions calculate the values of matrix B on all sides of the element.

4.1.13 assemble()

This function assembles the element stiffness matrix of each element to global element stiffness matrix.

4.1.14 solve()

This function solve the equations formed using the un-symmetric gauss elimination method.

4.1.15 iterate()

This function check if the velocities has converged to the required tolerance or not. If convergence is reached then it returns 1one to terminate the solution else return zero to continue with the neat iteration.

4.2 Computer Implementation of unsteady problem

Here functions of the program developed to study steady state problem are discussed.

4.2.1 main()

This function is the point from where program execution starts. It calls the following functions in the order mentioned; details of these functions are given in following sections:

- grid()
- H_CAL()
- POISSON_EQN()
- UV_CAL()
- NXT_STEP()

4.2.2 grid()

This function calculates the x and y coordinates of the grid points and stores them in an array. It also calculates the number of divisions in y direction corresponding to a particular x division and also stores it. To see if a grid point is outside the circular domain or not it in turn calls two functions, these are,

- y_cord()
- x_cord()

4.2.3 y_cord()

This function calculate the x coordinate of the point on the circle from which lines of constant y coordinates pass to check if a grid point is outside or inside the domain. It returns the value of the y coordinate of the point.

4.2.4 x_cord()

This function calculate the y coordinates of the points on the circle from which lines of constant x coordinates pass to check if grid points are outside or inside the domain.

4.2.5 H_CAL()

This function calculates the values of H1 and H2, the sum of advective and viscous terms. This function in turn calls three functions, these are,

- VERIFY()
- H()
- EXTRAPOLATE_H()

4.2.6 VERIFY()

This function checks for if there is need for a value to be extrapolated at the grid point or there are enough grid points around the grid point under the consideration to calculate the value of the variable at that point. It reruns one if there is need for values to be extrapolated at a grid point else it return zero.

4.2.7 H()

This function calculates the values of H1 and H2 at those grid points which have enough grid points around them. It calculated values are stores in an array.

4.2.8 EXTRAPOLATE_H()

This function extrapolates the values of the variables at those grid points which have not enough grid points around them to calculate the values at them. It extrapolates the values depending upon the values of the near grid points.

4.2.9 POISSON_EQN()

This function solves the Poisson equation. Pressure is calculated and stored in the array. The pressure is also compared with the old values and if it converges to the given limits then it finally terminates and stores the final pressure values. This function calls other functions in it to calculate various values, these are

- RHS_P()
- RHS_Q()
- EXTRAPOLATE_P()
- P_ITE()

4.2.10 RHS_P()

This function calculates the summation of the pressure terms formed by the discretization of the Poisson equation.

4.2.11 RHS_Q()

This function calculates the gradient of the H1 and H2 and returns the values to the function POISSON_EQN().

4.2.12 EXTRAPOLATE_P()

This function extrapolates the values of pressure at those grid points which have not enough grid points around them to calculate the pressure using the Poisson equation.

4.2.13 P_ITE()

This function compares the new values of the pressure with the old ones and sees if the required tolerance limits set are met or not. If the limits are met it returns one to indicate the termination of the pressure calculating process else it

stores the new pressure in place of old ones and returns zero to indicate the continuation of the loop to calculate pressure again.

4.2.14 UV_CAL()

This function calculates the values of the velocities at the new time step using the pressure calculated using the Poisson equation in the previous function and stores them in an array.

4.2.15 NXT_STEP()

This function replaces the initial guess of the velocities with the new values calculated as the initial guess for the velocities at the next time step.

CHAPTER 5

RESULTS AND DISCUSSION

5.1 Introduction

Based on the algorithms presented in chapter 3, computer programs both for the steady state and the unsteady Navier-Stokes equations have been developed. Details of these programs are discussed in chapter 4. The program for steady state equations gives the steady state flow pattern around the circular cylinder whereas program for the unsteady state equations gives the complete history of the development of the flow around the cylinder till the flow becomes fully developed. For both the problems flow pattern is studied at a Reynolds number of 20. The parameters associated with the program are,

Reynolds Number, Re= 20 (based on the cylinder's diameter).

Molecular viscosity, $\mu = 0.1$

Fluid density, $\rho = 1.0$

Free stream velocity, $u_\infty = 1.0$

Due to the symmetry of the flow only half of the domain of the flow is considered.

5.2 Flow Pattern for Steady Problem

For the steady state problem finite element method using residual Galerkin approach is used to discretize the equations. Iterative procedure is used to solve the equations. Some values of velocities are initially assumed and the pressure is calculated. Based on this pressure Navier-Stokes equations are solved which gives the velocities which are again used to calculate pressure and so on. The program runs until the velocities in both the directions are within the set tolerance limits. When the flow becomes stable, the final velocities are stored in a file and another program shows graphically the flow field. The flow field is shown in fig 5.1

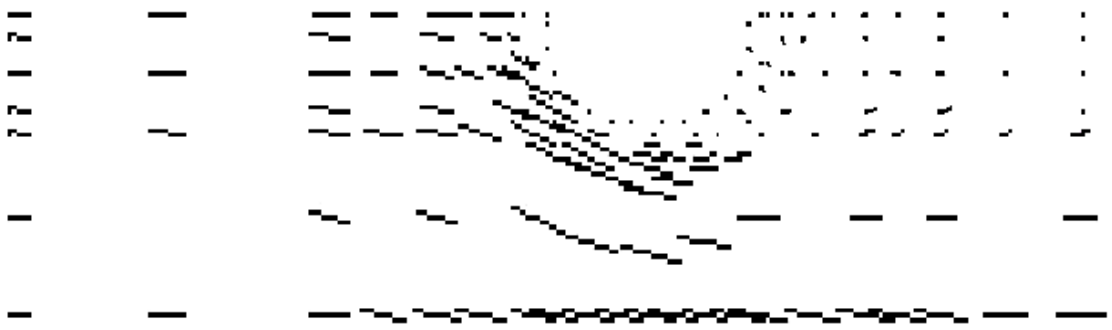

Fig 5.1 Flow Pattern for a steady state problem
(Result from the program)

Fig 5.2 Flow Pattern for a steady state problem
(As Interpreted)

Fig 5.2 shows the flow field. The flow is smooth over the surface of the cylinder. On the downstream a wake is formed which is stable and does not effect the flow further downstream i.e. it does not shed vortices. The wake is small in size and there is recirculation of the fluid in it.

The results presented here are in good agreement with the experiments conducted by various authors and the literature found. The results are also confirmed by the numerical study done by Taylor and Hughes [18] in which they used the finite element method and the residual Galerkin approach to solve the steady state Navier-Stokes equations. Fig 5.3 shows the profile of the

dimensionless velocity in x direction with the distance from the centre of the cylinder at the top of the cylinder.

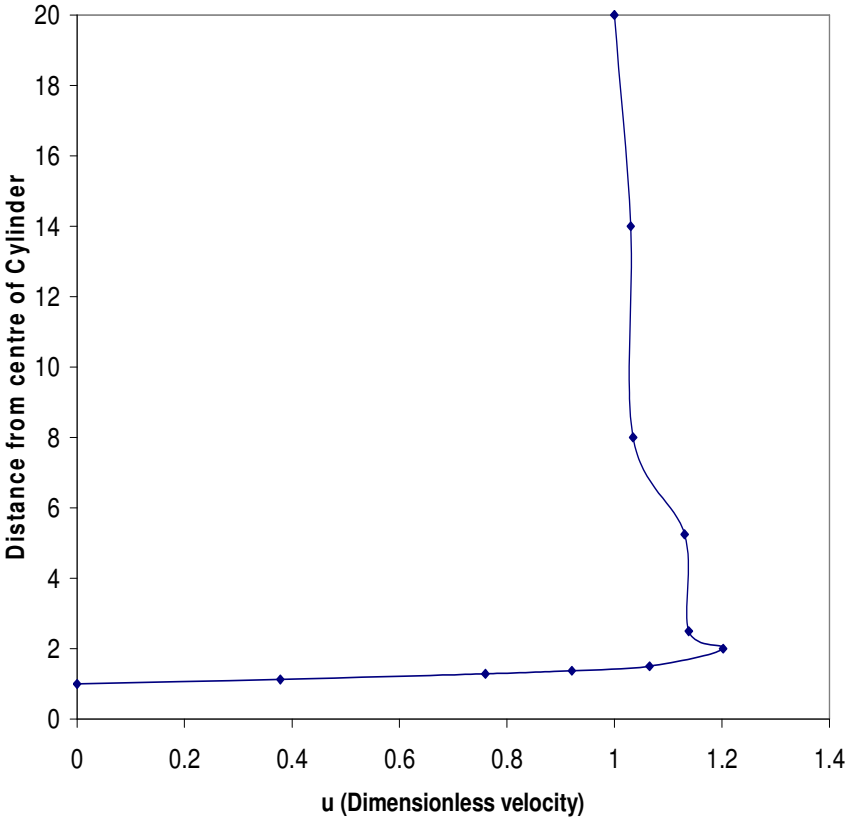

Fig 5.3 Velocity versus Distance from centre of cylinder

The profile of the velocity with distance at the center of the cylinder shown above is also is in good agreement with the velocity profile results of the Hughes and Taylor. Hence the steady state results are in good agreement with the literature surveyed.

5.3 Flow Pattern for Unsteady Problem

In the previous section flow pattern for the steady state problem is discussed at Reynolds number 20. In this section flow pattern for the unsteady problem is discussed. In the unsteady problem, complete history of the flow pattern is available at different time steps.

For the problem time step of 0.05 is chosen. After dimensionless time 0.5, the velocities are collected and the flow pattern is viewed. Below Fig. 5.4 shows the flow pattern at various time intervals. For the flow pattern below it is clear that at initially at time interval 0.5, the flow is smooth around the cylinder. There are no any traces of wake behind the cylinder and also there is not any recirculation of flow around the cylinder. At time interval of 1.0 there is some increase in the velocity in the upstream of the cylinder near the outer surface of the cylinder but there are not any traces of wake formation indicating initially the flow is smoothly divides and reunites around the cylinder.

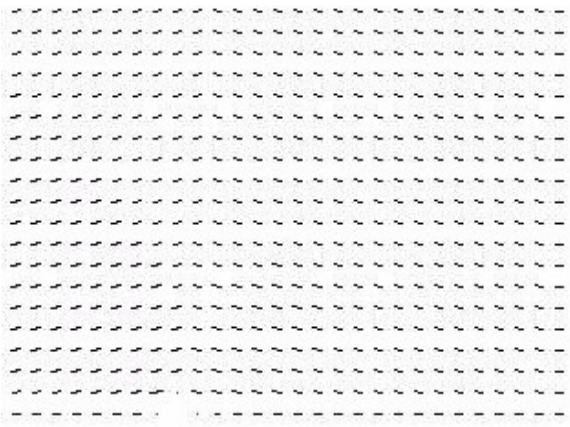

Flow Pattern at time t = 0.5

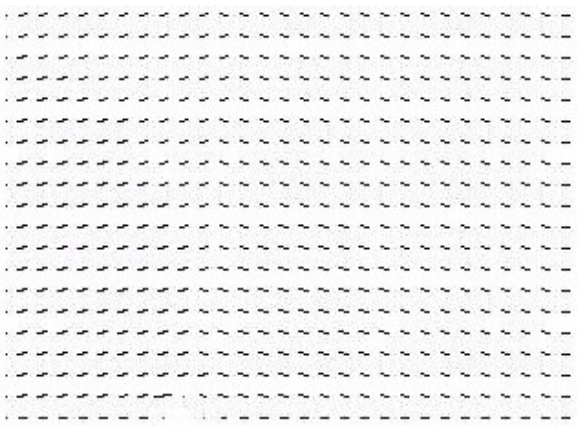

Flow Pattern at time t = 1.0

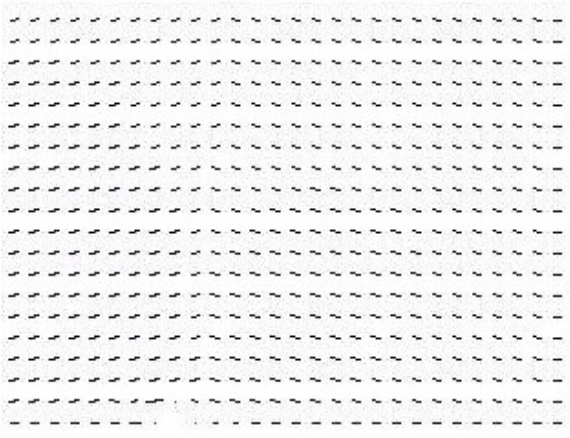

Flow Pattern at time t = 1.5

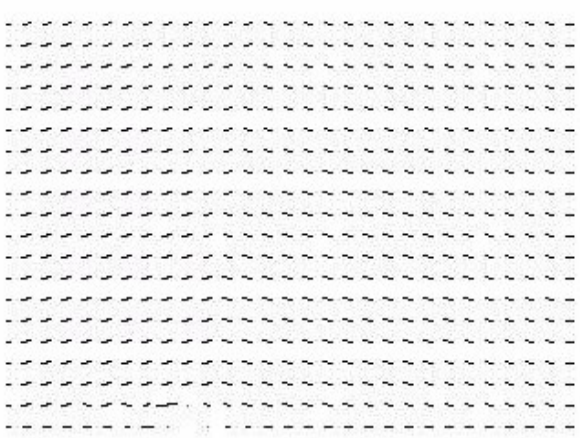

Flow Pattern at time t = 2.0

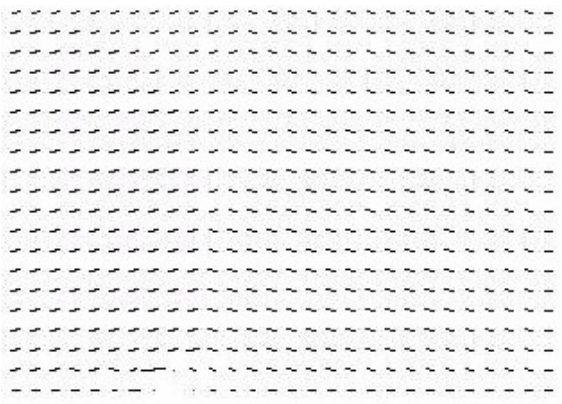

Flow Pattern at time t = 2.5

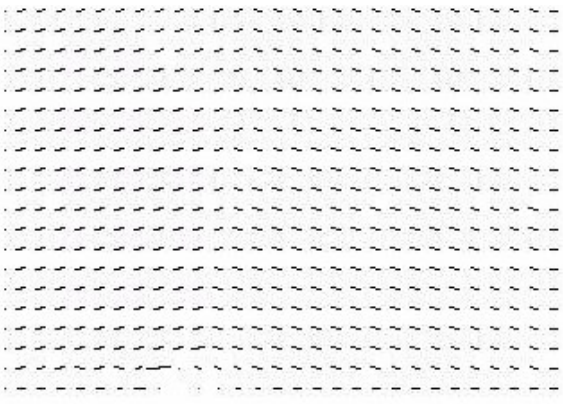

Flow Pattern at time t = 3.0

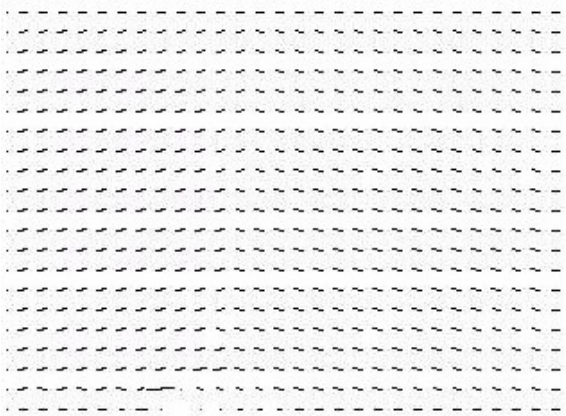

Flow Pattern at time t = 3.5

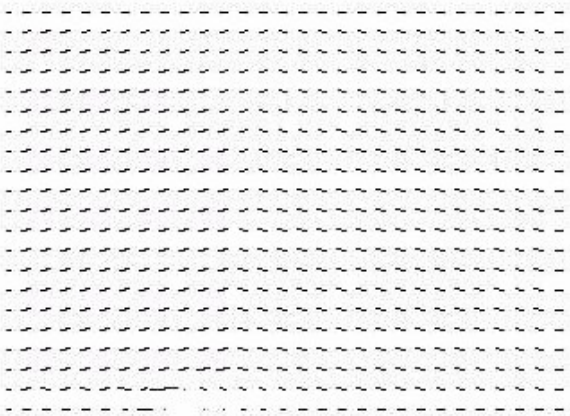

Flow Pattern at time t = 4.0

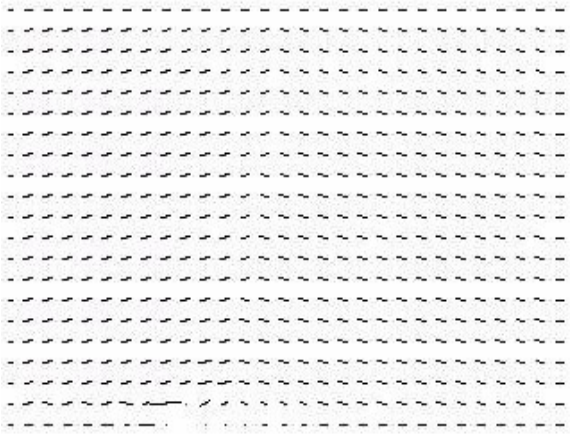

Flow Pattern at time t = 5.0

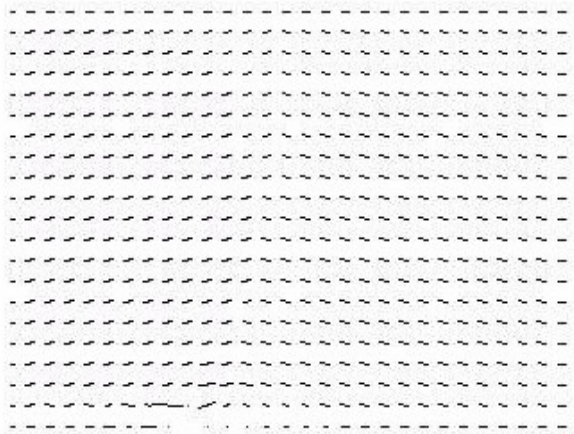

Flow Pattern at time t = 5.5

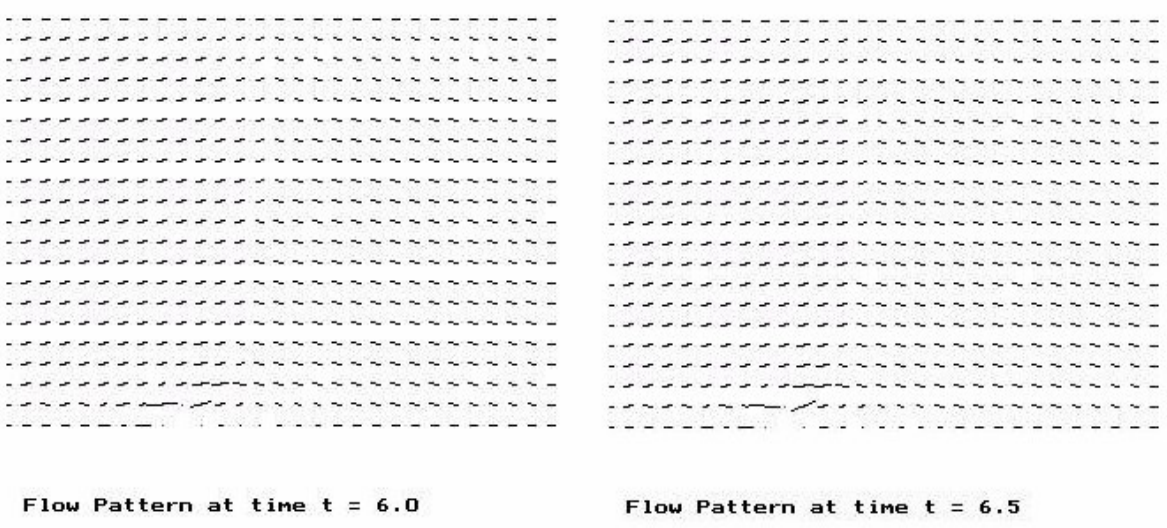

Fig 5.4 Flow Pattern at Various Time Intervals (Time is Dimensionless)

Now at time interval 1.5, there are indications of the formation of the wake behind the cylinder and tendency of reversal of flow at the back of the cylinder. At time interval 2.0 and 2.5, there is a greater negative value of velocity indicating the reversal of flow indicating the formation of the wake and the re-circulation region in the near vicinity of the cylinder. At time intervals 3.0, 3.5 and 4.0 the same trend continues and there is a development of the re-circulation region. At 5.0 and 5.5, the region increases a little further downstream and also there is little increase in velocity of the flow on the top of the cylinder. At time 6.0, the wake has developed fully and also there is a recirculation region in the near vicinity of the cylinder. At time interval 6.5, the flow has become nearly stable and the wake now is fully formed and also there is a recirculation region. As in the unsteady state problem, the wake remains near the near the vicinity of the cylinder which is stable and is not carried downstream with the flow.

Now the results presented here are in agreement with the results of the study conducted by Braza et al. [4] on the unsteady incompressible flow around the cylinder using second order finite volume method. They found that at

Reynolds number of 20 the flow reaches the steady state at about time near to t=7 and two attached vortices are formed behind the cylinder as in our case.

Fig 5.5 shows the profile of the dimensionless velocity in x direction with the distance from the centre of the cylinder at the top of the cylinder at time t=6.5.

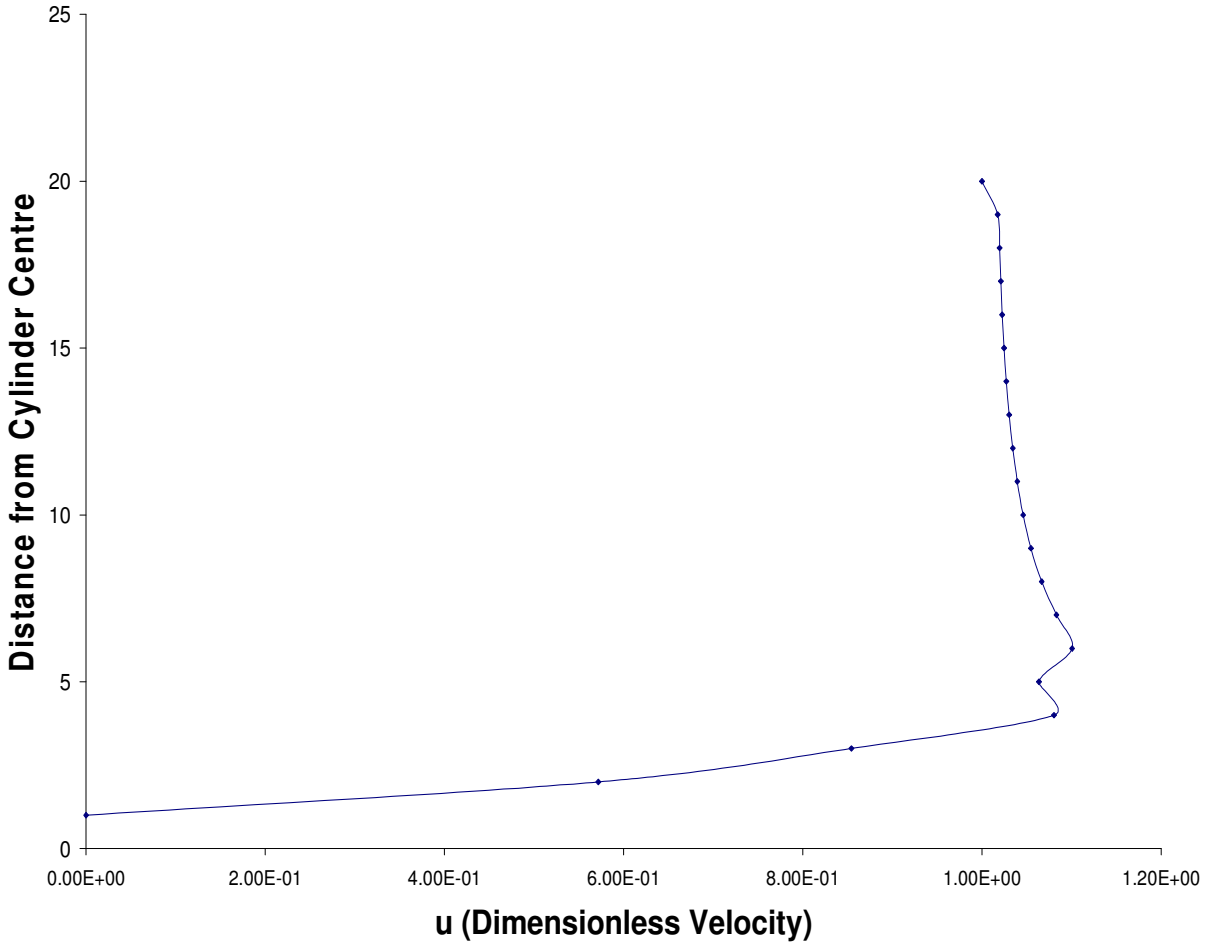

The graph shown above represents the dimensionless velocity in x-direction with distance from the axis of the cylinder at the top surface of the cylinder. The variation of the velocity in unsteady state at t=6.5, is nearly the same as the variation of the velocity in the steady state which are further validated by Hughes and Taylor [18].

CHAPTER 6

CONCLUSION AND SCOPE OF FUTURE WORK

In the present work both steady and unsteady flow around a circular cylinder is studied at Reynolds number of 20. Navier-Stokes equations and the continuity equation in dimensionless form and in the velocity-pressure formulation are considered for the study of the both steady and unsteady flow problem. Finite element method using residual Galerkin approach is used to solve the flow problem in steady state and the results are matched with the existing calculations done by various researchers. An explicit time marching scheme of approximate factorization for the solution of unsteady Navier-Stokes equations for the velocity field is used while the pressure field is computed from Poisson equation in which a time step of 0.05 is used. The advantage of the unsteady solution is that it gives the complete history of the flow pattern till the flow becomes fully developed and it helps in determining wake characteristics. From the steady state calculations it can be concluded that at Reynolds number 20, the flow separates in the downstream and two symmetrical wakes are formed in near the vicinity of the cylinder. The wakes remain attached to the cylinder and are not conveyed further downstream. Outside this region the flow remains steady. The wakes formed are steady and do not grow in size. Also for the unsteady problem, two symmetrical wakes are formed on both the sides of the cylinder. The wakes remain attached to the cylinder from the start till the flow becomes fully developed and does not affect the flow further downstream. Also the time taken by the solution to become fully developed is nearly the same as reported in the previous papers and after the full development of the flow the results of unsteady state are in agreement with those of the steady state solutions.

Scope of future work:

In the present work Reynolds number of 20 is considered, the work can further enhanced by the following ways:

- Present work is done only at Reynolds number of 20, so work can be done at different Reynolds number to see how the flow behaves as Reynolds number is changed.
- At Reynolds number becomes 40, vortices start to oscillate in time. This can be studied in detail if Strouhal number if considered.
- Here explicit time advancing scheme is used, there are other schemes which are discussed but not implemented, which needs to be worked with.
- For unsteady problem finite difference method is considered, work is need to be done to solve the unsteady problem using finite element method.
- Variation of coefficient of drag and lift with Reynolds number needs to be studied and factors which influence coefficient of drag and leads to its reduction be probed in greater detail.

REFERENCES

1. Bearman PW, “On Vortex Shedding from a Circular Cylinder in the critical Reynolds number Regime”, Journal of Fluid Mechanics, Vol. 37, pp. 577-585 (1969).
2. Bearman PW, Graham JMR, “Vortex Shedding from Bluff Bodies in Oscillatory Flow: A Report on Euromech 119”, Journal of Fluid Mechanics, Vol. 99, part 2, pp. 225-245 (1980).
3. Berger E, Willie R, “Periodic Flow Phenomenon”, Annual Review of Fluid Mechanics, Vol. 4, pp. 313 (1972).
4. Braza M, Chassaing P, Ha Minh H., “Numerical Study and Analysis of the Pressure and Velocity Fields in the Near Wake of a Cylinder”, Journal of Fluid Mechanics, Vol. 165, pp. 79-130 (1986).
5. Ferziger H. Joel, Perii Milovan, “Computational Methods for Fluid Dynamics”, Second Edition, Springer, (1999).
6. Friehe A, “Vortex Shedding from Cylinders at Low Reynolds Numbers”, Journal of Fluid Mechanics, Vol. 100, pp. 237-241 (1980).
7. Gaster M, “Vortex Shedding from Circular Cylinders at Low Reynolds Number”, Journal of Fluid Mechanics, Vol. 46, pp. 749-761 (1971).
8. Griffin M. Owen, “Vortex Streets and Patterns”, Mechanical Engineering, pp.56-61, (March 1982).
9. Hammache M, Gharib M, “An Experimental Study of the Parallel and Oblique Vortex Shedding from Circular Cylinders”, Journal of Fluid Mechanics, Vol. 232, pp. 567-590 (1991).
10. Jackson C.P., “A Finite Element Study on the onset of Vortex shedding in flow past variously shaped bodies”, Journal of Fluid Mechanics, Vol. 182, pp. 23-45 (1987).
11. Jong Youb SA, Kenu Shik Chang, “Shedding Pattern of the Near Wake Vortices behind a Circular Cylinder”, Int. J. for Numerical Methods in Fluids, Vol. 12, pp. 463-474 (1991).

12. Lee T, Budwig R, “A Study of the Effect of Aspect Ratio on Vortex Shedding Behind Circular Cylinders”, Physics of Fluids A, Vol. 3, pp. 309-314 (1991).
13. Mair WA, Stansby PK, “Vortex Wakes of Bluff Cylinders in Shear Flow”, SIAM Journal of Applied Mathematics, Vol. 28, pp. 519-539 (1975).
14. Maull DJ, Young RA, “Vortex shedding from Bluff Bodies in a Shear Flow”, Journal of Fluid Mechanics, Vol. 60, pp. 401-413 (1973).
15. Mukhopadhyay A, Venugopal P, Vanka SP, “Numerical Study of Vortex Shedding From a Circular Cylinder in Linear Shear Flow”, Transactions of the ASME, Vol. 121, pp. 460-468 (1999).
16. Noberg C, “An Experimental Investigation of the Flow around a Circular Cylinder: Influence of Aspect Ratio”, Journal of Fluid Mechanics, Vol. 258, pp. 287-316 (1994).
17. Ozisik Neccati M., “Finite Difference Methods in Heat Transfer”, CRC Press, (1995).
18. Perry AE, Chong MS, Lim TT, “The Vortex Shedding Process Behind Two-Dimensional Bluff Bodies”, Journal of Fluid Mechanics, Vol. 116, pp. 77-93 (1982).
19. Taylor C, Hughes T.G., “Finite Element Programming of Navier-Stokes Equations”, Pineridge Press Limited., (1981).
20. Triantafyllou GS, Triantafyllou MS, Chryssostomidis C, “On the Formation of Vortex Shedding Behind Stationary Cylinders”, Journal of Fluid Mechanics, Vol. 170, pp. 461-477 (1986).
21. Tritton DJ, “A Note on Vortex Streets behind Circular Cylinders at Low Reynolds Numbers”, Journal of Fluid Mechanics, Vol. 45, pp. 203-215(1971).
22. Wen CY, Lin CY, “Two-Dimensional Vortex Shedding of a Circular Cylinder”, Physics of Fluids, Vol. 13, pp. 557-560 (2001).
23. Williamson CHK, “The existence of two stages in the transition to three-dimensionality of a cylinder wake”, Physics of Fluids, Vol. 31, pp. 3165-3168 (1988).

24. Williamson CHK, “Defining a Universal and Continuous Strouhal-Reynolds Number Relationship for the Laminar Vortex Shedding of a Circular Cylinder”, Physics of Fluids, Vol. 31, pp. 2742-2744 (1988a).
25. Williamson CHK, “Oblique and Parallel Modes of Vortex Shedding in the Wake of a Circular Cylinder at Low Reynolds Numbers”, Journal of Fluid Mechanics, Vol. 206, pp. 579-627 (1989).
26. Williamson CHK, “Vortex Dynamics in the Cylinder Wake”, Annual Review of Fluid Mechanics, Vol., pp. 477-539 (1996).
27. Zhang H, Fey U, Noack BR, König M, Eckelmann H, “On the transition of the Cylinder Wake”, Physics of Fluids, Vol. 7, pp. 1-5 (1995).